AEROSOL EFFECTS ON SATELLITE RETRIEVALS OF CLOUD OPTICAL PROPERTIES IN THE SOUTH ATLANTIC OCEAN

By

K. ELENA WILLMOT

A thesis submitted in partial fulfillment of

the requirements for the degree of

Master of Science

(Atmospheric and Oceanic Sciences)

at the

UNIVERSITY OF WISCONSIN-MADISON

2014

APPROVED

Advisor Title:

Ralf Bennartz, Ph.D.

University of Wisconsin – Madison

Department of Atmospheric and Oceanic Sciences

_____

Advisor Signature

_____

Date

ABSTRACT

Satellite retrievals of cloud optical depth and effective radius are shown to be underestimated in the South Atlantic Ocean, where biomass-burning aerosols typically reside above low-level, liquid water stratocumulus clouds. A radiative transfer model is used to calculate top of the atmosphere (TOA) reflectances for a case where an aerosol layer is elevated above a liquid cloud in the South Atlantic Ocean. Both absorbing and scattering aerosols are modeled at varying aerosol optical depths (AOD) at 0.86 μm and 2.10 μm. Optimal estimation methods are used to convert reflectance pairs into a retrieved cloud optical depth and effective radius, similar to the Moderate Resolution Imaging Spectroradiometer (MODIS, aboard Aqua satellite) algorithm. Absorbing aerosols lead to an underestimation of the retrieved cloud optical depth by up to 60 – 80%, while scattering aerosols can lead to an over- or underestimate of the optical depth by up to 10%, depending on the cloud thickness. Effective radius retrievals can be over- and underestimated if absorbing aerosols are present, depending on the AOD. Scattering aerosols result in an overestimation of effective radius by up to 0 – 10%. A-Train satellite observations from August 2006 – December 2010 in the South Atlantic Ocean also show that the MODIS biases in cloud optical depth and effective radius are likely affecting retrieved properties and hence retrieved cloud droplet number concentrations when the aerosol layer is vertically separated from the cloud.

ACKNOWLEDGEMENTS

This work would not have been possible were it not for Dr. Ralf Bennartz and his mentorship and support throughout my career. I would like to thank John Rausch for his continued technical support, and his assistance with various programming tasks. I would also like to thank my readers, Dr. Steve Ackerman and Dr. Tristan L'Ecuyer for their comments and suggestions. The University of Wisconsin Department of Atmospheric and Oceanic Sciences has been truly spectacular to be a part of, and I am thankful for my continued support from various faculty, staff and students. A special thank you to my parents, Pat and Doug Willmot, along with my brother, Russell, for their encouragement, advice, and motivation as I've navigated my undergraduate and graduate careers. Finally, I need to thank my closest friend, Alex Karambelas, and boyfriend Croix Christenson for their support and assistance with the ideas and execution behind this thesis.

The CALIPSO data used in this study were acquired from NASA's Langley Research Center; the CloudSat data were acquired from the CloudSat Data Processing Center; the Aqua MODIS data were acquired from the Goddard Earth Sciences Data and Information Services Center (GES DISC). Data were processed by the A-Train Validation of Aerosol and Cloud properties from SEVERI (AVAC-S) developed at the European Organisation for the Exploitation of Meteorological Satellites (EUMETSAT).

TABLE OF CONTENTS

1. Introduction

1.1 Background

The energy balance of the Earth is the driving factor in climate dynamics, and understanding the processes by which the energy balance is altered is critical to understanding the climate system. Clouds as well as atmospheric gases and particles can have profound impacts on the energy balance in different ways and varying magnitudes. The radiative impacts of aerosols and clouds and the complex interactions between the two remain the most dominant source of uncertainty in climate modeling (Boucher et al., 2013; citations therein; Forster and Ramaswamy, 2007). Global anthropogenic air pollution adds a variety of aerosols into the atmosphere including black carbon (BC), sulfate, nitrate, and ammonium on the order of tens of Tg yr^{-1} (Boucher et al., 2013; citations therein). Aerosols scatter and absorb radiation at different wavelengths, and each type of aerosol interacts differently. Certain aerosols have the ability to take up water in more humid environments, which changes their radiative effect. This also allows hygroscopic aerosols to be activated as cloud condensation nuclei (CCN) under specific supersaturated conditions. Thus, aerosols that act as cloud condensation nuclei have complex interactions with the microphysical properties of clouds based on the cloud phase. This study focuses on low level, liquid water clouds, specifically stratocumulus clouds.

Stratocumulus clouds cover vast areas of ocean, most often occurring in subtropical regions that experience strong subsidence. They typically cover one-fifth of the Earth's surface (23% of the ocean surface and 12% of the land surface) in the annual

mean which makes them exceptionally important for the Earth's energy balance (Wood, 2012). Stratocumulus clouds can persist for long periods of time as they receive abundant moisture from oceans below, which is then mixed throughout the boundary layer via turbulence (Figure 1.1). In covering such a large area, these clouds will have an obvious effect on the Earth's radiation budget, and therefore, global climate, by reflecting solar radiation back into space and cooling the earth. This effect can vary depending on cloud microphysical properties, such as cloud optical thickness and droplet effective radius. It is well understood that clouds with high aerosol concentrations will contain more cloud droplets at smaller sizes which can, in turn, reflect more sunlight back to space, thereby cooling the Earth (Twomey et al., 1984). This is also known as the first aerosol indirect effect (or the cloud albedo effect), and has a negative radiative forcing (cooling effect).

Aerosols can also lead to a positive radiative forcing via the semi-direct effect, or the cloud lifetime effect. Absorbing aerosols such as soot (BC) heat the air and decrease the local relative humidity, which then decreases low cloud amounts. However, the magnitude of this effect is sensitive to the type of aerosol (scattering versus absorbing), and the vertical distribution of the aerosol with respect to the low cloud. Johnson et al. (2004) find that absorbing aerosols within the marine stratocumulus boundary layer exhibit a much larger semi-direct effect (almost twice the magnitude) than absorbing aerosols above the boundary layer. Scattering aerosols above the boundary layer experience a negative semi-direct effect, as they tend to reduce the temperature and raise the relative humidity locally. This scenario quickly becomes complicated when there are a variety of aerosol types residing above the cloud and within it, thus changing the cloud microphysics and radiative properties.

This study focuses on the region over the South Atlantic Ocean off the west coast of Angola and Namibia (Figure 1.2). Frequent, persistent, and large stratocumulus cloud decks characterize this region throughout the year. In western Africa, millions of square kilometers of vegetation are burned every year (Roberts et al., 2009) and mean easterly winds advect plumes of smoke and aerosols out over the southern Atlantic Ocean, thus the interaction between aerosols and clouds in this region is of particular interest. The widespread burning of vegetation in Africa, known as biomass burning, releases a combination of BC, organic compounds, ammonium, nitrate, and sulfate into the air on the order of 23.9 Tg yr^{-1} (Table 1.1 from Boucher and Randall, 2013). Africa also emits anthropogenic sulfur dioxide, a hygroscopic scattering aerosol, at 3.1 TgS yr^{-1} on average. Sulfates typically form when sulfur dioxide, or other sulfur-based gases, that is emitted from anthropogenic sources, such as electricity-generating units, becomes oxidized in the atmosphere. Both sulfates and soot are prevalent in the atmosphere over Africa, thus this study uses both aerosol types to compare the effects of a scattering (sulfate) and absorbing (soot) aerosol on satellite retrievals of stratocumulus cloud properties.

1.2 Satellite Retrievals of Clouds and Aerosols

The NASA A-Train satellite constellation consists of several Earth-observing satellites that follow one another along an orbital track. The satellites are polar-orbiting, and they cross the equator at 1:30pm local time, which warrants the name "Afternoon Constellation" or A-Train. The satellites follow one another closely, allowing for near-simultaneous observations of a number of environmental parameters. Several of the

satellites are used for cloud and aerosol observations, including CloudSat, Cloud-Aerosol Lidar and Infrared Pathfinder Satellite (CALIPSO), and Aqua.

CloudSat was launched in 2006 in hopes of providing more detailed cloud observations, including liquid and ice contents, vertical structure, and their global distribution. CloudSat houses a 94 GHz nadir-looking radar, called the Cloud Profiling Radar (CPR). The CPR has a vertical resolution of 500 m (from the surface to 30 km), a cross-track resolution of 1.4 km, and an along-track resolution of 1.7 km. CloudSat lags Aqua by less than 120 s and leads CALIPSO by 15 s (Stephens et al., 2002). The CloudSat radar measurements, combined with radiances from the other A-Train satellites, provide a more complete picture of global low water clouds (Stephens et al., 2002).

CALIPSO is a joint NASA and Centre National d'Études Spatiales (CNES) mission aiming at improving our understanding of the role of aerosols and clouds on the Earth's climate. CALIPSO houses an active polarization-sensitive lidar, called the Cloud-Aerosol Lidar with Orthogonal Polarization (CALIOP), which is used to detect cloud and aerosol features. CALIOP has a 30-60 m vertical resolution and a 333 m horizontal resolution. Two channels measure orthogonally polarized backscattered radiation at 532 nm in the visible part of the spectrum, and one channel measures backscatter intensity at 1064 nm in the infrared. The CALIPSO Cloud and Aerosol Layer products are determined using a threshold algorithm which inputs profiles of 532 nm attenuated scattering ratio data (Vaughan et al., 2005). If the backscatter values exceed some threshold "clear air" value, a feature is detected (clouds, aerosols, surfaces, i.e.). An algorithm, outlined in Vaughan et al. (2005), separates the features and determines their spatial extent. An example of a CALIOP vertical profile for the South Atlantic Ocean is

shown in Figure 1.3 from September 15, 2007. The backscatters at 532 nm show a low stratus cloud deck at 1 km with a layer of aerosols between 2 and 5 km. The Vertical Feature Mask points out the individual features that were detected by the algorithms.

Aqua leads the A-Train constellation and has six different Earth-observing instruments on board. Those that are relevant to this study are the Moderate Resolution Imaging Spectroradiometer (MODIS), and Advanced Microwave Scanning Radiometer for the Earth Observing System (AMSR-E). AMSR-E is a passive microwave sensor used to obtain cloud liquid water content (among other properties). MODIS is a passive radiometer that operates at 36 spectral bands from 0.4 to 14.4 μm with each band being useful for detection of different parameters (ozone, carbon dioxide, water vapor, etc). The along-track resolution is 10 km and the cross-track resolution is 2330 km, covering the entire Earth every one-two days. MODIS uses reflectances at a combination of water-absorbing bands (1.6, 2.1, or 3.7 μm) and water non-absorbing bands (0.65, 0.86, or 1.2 μm) to obtain cloud optical properties such as the optical depth and effective radius (Platnick et al., 2003). The default water-absorbing band is 2.1 μm, and the default non-absorbing band over oceans is 0.86 μm, and these two channels comprise the main bands throughout this study. When obtaining the cloud properties, MODIS neglects any overlying aerosols which has been shown to bias the retrievals (Cattani et al., 2006; Haywood et al., 2004; Meyer et al., 2013). This study uses a radiative transfer model and A-Train observations to show the effects of varying aerosol layer thicknesses and aerosol types on MODIS retrievals of low, liquid cloud properties.

1.3 Satellite Observations in the South Atlantic Ocean

Devasthale and Thomas (2011) use the CALIPSO Cloud and Aerosol Layer products to show that there is a strong seasonality in events where biomass burning aerosols reside over low, liquid water clouds. The frequency of these events peaks in September, October, and November over the Atlantic Ocean near the west coast of Africa. In 5-10% of all global overlap events (where aerosols reside over low liquid water clouds), the distance between the aerosol layer and cloud deck is less than 100 m, while in 50% of the cases, the aerosols reside between 2 and 4 km. Wilcox (2010) uses the same Cloud and Aerosol Layer products to show that the layer of biomass burning aerosols typically resides between 2 and 4 km, and the low clouds are usually below 1 km (Figure 1.4). This distinct separation of aerosols from the cloud has a significant impact on the radiative balance in this region, producing a net positive radiative forcing (Wilcox, 2012) and thus, a warming effect. Thus, the scenario in which aerosols overlie liquid water clouds is important in determining the net radiative effect of the system as a whole.

The 532 nm wavelength attenuates faster than the 1064 nm wavelength due to the scattering properties of aerosols and clouds, and it also experiences significant noise from solar reflection. This is mostly true in the daytime when solar radiation is scattered back towards the sensor at 532 nm. This will cause the 532 nm backscatter data to underestimate the amount of aerosols in the vicinity of the cloud, thus creating a bias in the number of cases where aerosol layers touch the clouds. The observational portion of this study uses the 1064 nm backscatter profiles to determine whether or not aerosol layers touch the cloud and what effect that will have on the cloud droplet number

concentrations. This will minimize the solar noise issues observed at 532 nm, and allow daytime observations to be used with more accuracy.

1.4 Figures

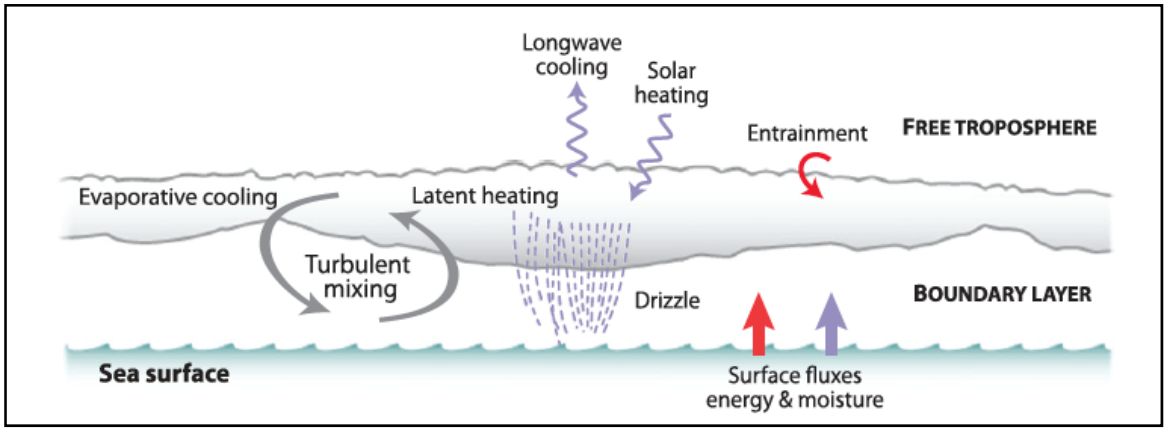

Figure 1.1: Schematic showing processes involved in a stratocumulus layer *(Fig. 2 from Wood, 2012).*

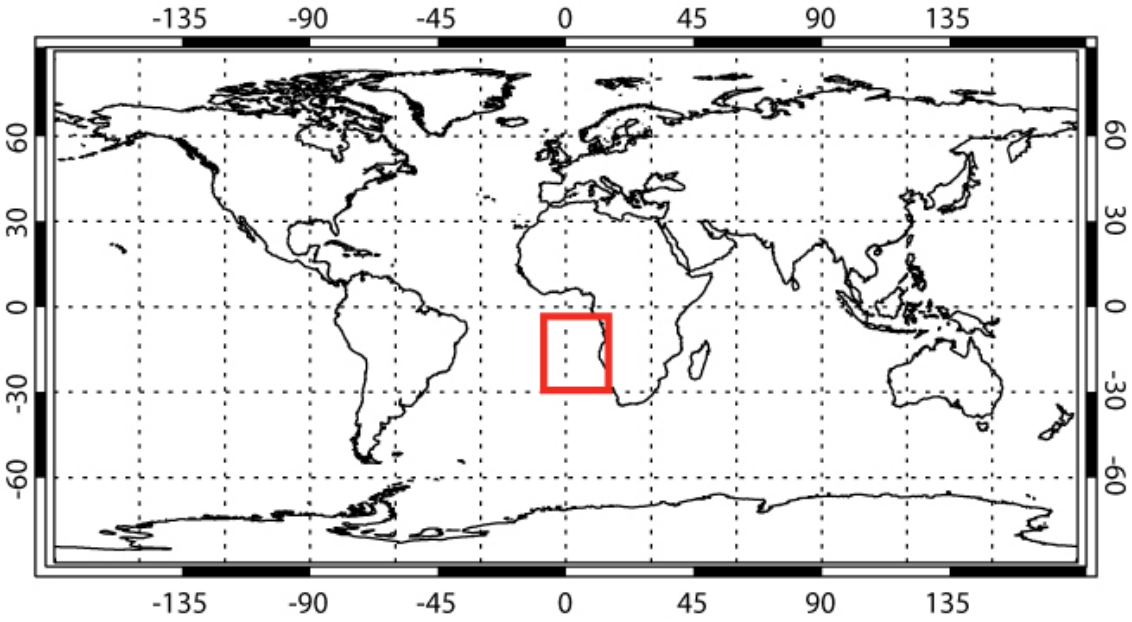

Figure 1.2: Area of interest in South Atlantic Ocean off west coast of Namibia and Angola. Area is defined as 5.0°S to 30.0°S and 10°W to 15°E.

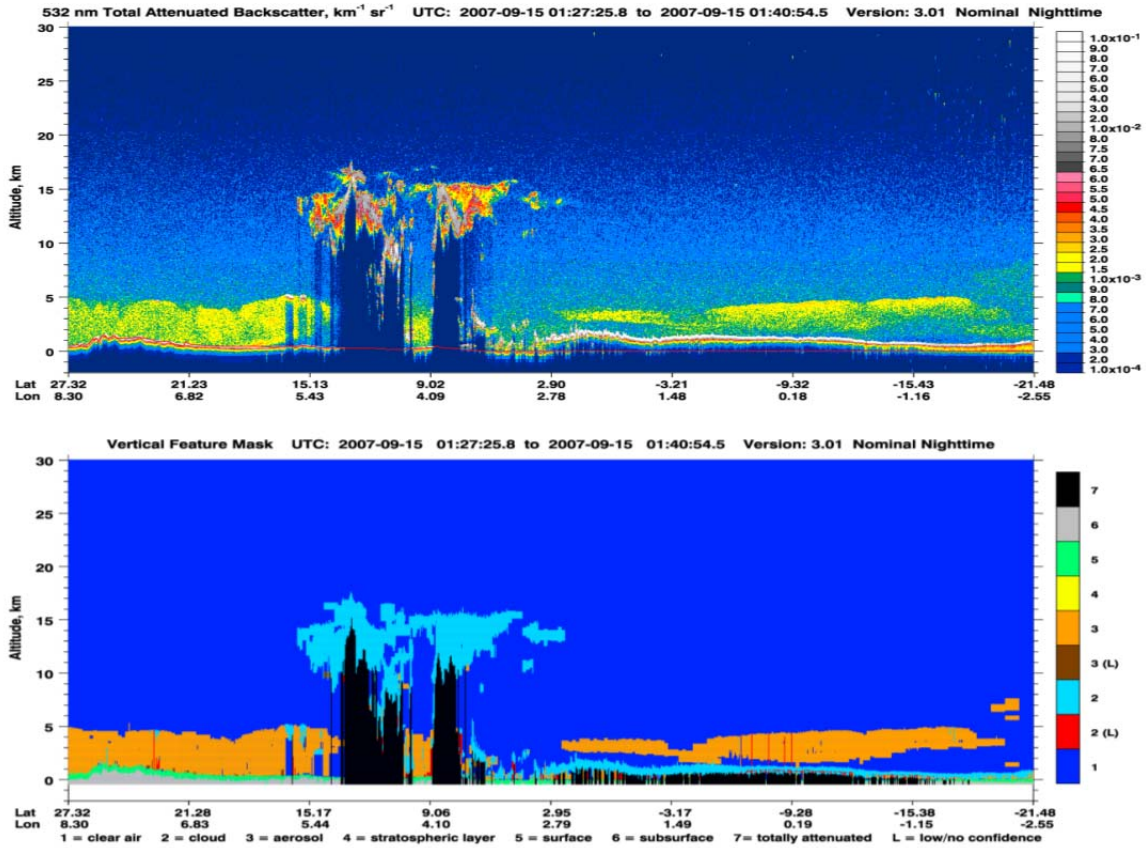

Figure 1.3: Vertical profile from a transect of a CALIOP overpass over the South Atlantic Ocean September 15, 2007. The 532 nm total attenuated backscatter in km^{-1} sr^{-1} (top panel) depicts a stratus cloud at 1 km with an overlying aerosol layer (right half of image). The bottom panel shows the Vertical Feature Mask, which detects the cloud and overlying aerosol layer using the 532 nm backscatter values. (*Images from http://www-calipso.larc.nasa.gov*.)

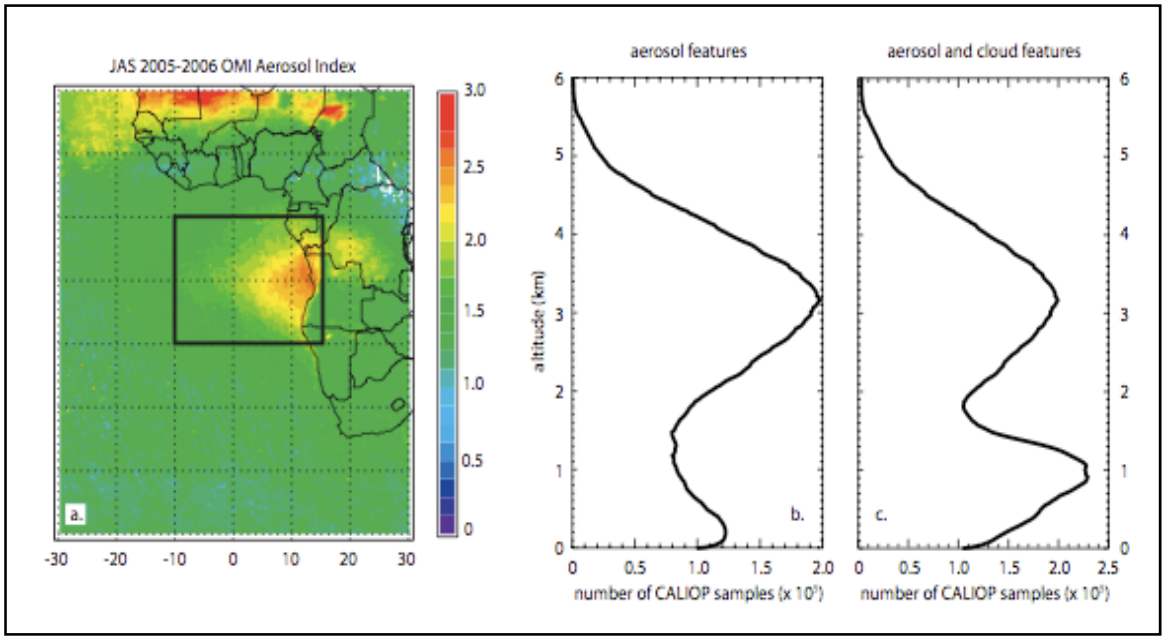

Fig 1.4: (Left) Aerosol Index from Aura's Ozone Monitoring Index (OMI) in area of interest. (Middle) Cloud-Aerosol Lidar with Orthogonal Polarization (CALIOP) aerosol feature. (Right) Combined CALIOP aerosol and cloud features. *From (Wilcox, 2010).*

2. Datasets and Methods

To investigate the effects of different aerosols (absorbing or scattering) on underlying cloud optical property retrievals, observational data from the A-Train satellites are compared to output from a radiative transfer model. The radiative transfer model, called Streamer, incorporates spectral optical properties for clouds, soot, and sulfates from the Optical Properties of Aerosols and Clouds (OPAC) dataset (Hess et al., 1998). Reflectances are modeled for a maritime stratus cloud with no overlying aerosol, and with an overlying aerosol of increasing aerosol optical depth (AOD). Optimal estimation is then used to convert the modeled reflectances, including the aerosol layer, to a retrieved cloud optical depth, τ', and effective radius, r_e'.

Data from the A-Train satellites are used to verify this effect with observations. A software system called the A-Train Validation of Aerosols and Clouds with SEVERI (AVAC-S) is used to collect the data from several satellites onto a common grid, resulting in several vertical profiles with measured cloud and aerosol properties. The Streamer model, OPAC dataset, AVAC-S software, and optimal estimation method are all described in detail in this section.

2.1 Streamer radiative transfer model

The radiative transfer model used in this experiment is called Streamer (Key and Schweiger, 1998), which uses a two-stream, discrete ordinate approximation method. Streamer uses a total of 129 bands; 24 of which are shortwave bands and 105 are longwave bands. The bands range from 500 micrometers in the far IR to 0.28 micrometers in the ultraviolet range. A number of important components of interest to

radiative transfer calculations are built-in and can be specified by the user. These include seven standard atmospheric profiles ranging from tropical to arctic winter, six optical models for aerosols (tropospheric, maritime, etc), absorption of gases (hydrogen, oxygen, ozone, carbon dioxide, and trace gases), as well as spectral albedos for a variety of surface types (dry sand, freshwater, etc). The calculations done for this experiment include gaseous absorption, assume no background tropospheric or stratospheric aerosols, and a completely oceanic surface type for the region of interest (see Fig. 1.2). The surface temperature is chosen to be that of the lowest atmospheric layer, as defined by the specified atmospheric profile. The atmospheric temperature profiles are determined by month and latitude as shown in Table 2.1.

A simulation with a maritime stratus cloud is run at 20°N and 0°E using tropical temperature and humidity profiles and neglecting all background aerosols. Several combinations of τ and r_e are computed. Simulations are run in Streamer for two channels encompassing either the 0.86 μm or the 2.1 μm wavelengths. The first channel ranges from 0.78 – 0.87 μm and the second ranges from 1.64 – 2.13 μm. For each simulation, the top of the atmosphere (TOA) radiance in W m^{-2} sr^{-1}, denoted $I^{\uparrow}$, is converted to a reflectance using the following equations from Petty (2006)

$$r_{0.86} = \frac{\pi I^{\uparrow}}{F_0 \cos(\theta_i)}, F_0 = 93.06992\ Wm^{-2}, \theta_i = 20°$$

$$r_{2.1} = \frac{\pi I^{\uparrow}}{F_0 \cos(\theta_i)}, F_0 = 19.13\ Wm^{-2}, \theta_i = 20°$$

where F_0 is the solar constant determined by Streamer for each band, and the solar zenith angle, θ_i, is 20.0°.

Combinations of reflectances at 0.86 and 2.1 μm are used to create lookup tables (LUT) of cloud optical depth and effective radius (see Fig. 4.1). A soot or sulfate layer is then placed above the cloud top, and the aerosol optical depth is gradually increased. The results are shown in Section 3. Section 4 discusses the sensitivity tests that were performed in order to investigate any possible sources of error in the radiative transfer experiments, which include the effects of different temperature profiles on the retrievals, the placement of the aerosol layer in the vertical, and the number of streams used in the calculations.

2.2 Optical Properties of Aerosols and Clouds (OPAC) Dataset

Developed in 1998, the OPAC dataset contains microphysical and optical properties of water droplets, ice crystals, and aerosol particles at several wavelengths in the solar and terrestrial spectral range (Hess et al., 1998). For this study, optical properties for two aerosol types are used (soot and sulfates), as well as data for a maritime stratus cloud. Water droplets and aerosols are assumed to be spherical. Optical properties are provided for eight different humidity conditions for water droplets and hygroscopic aerosols. In this study, the optical properties for sulfates, the only hygroscopic aerosol used, are assumed to be in a condition of 80% relative humidity.

The volume extinction coefficient, single scattering albedo, and asymmetry parameter are given for 61 wavelengths, ranging from 0.25 μm to 40 μm (Figure 2.1). The volume extinction coefficient, β_e, describes the attenuation of electromagnetic radiation due to both scattering (β_s) and absorption (β_a) by the medium.

$$\beta_e = \beta_a + \beta_s$$

β_e is scaled to be 1.0 km^{-1} at 0.6 μm, as that is Streamer's reference wavelength. The total amount of aerosol is then determined by the optical depth at 0.6 μm. As in the top panel of Figure 2.1, the marine stratus cloud is characterized by significant extinction throughout the spectrum, with some variability in the near infrared. Both aerosols have much higher extinction at shorter wavelengths in the visible, and gradually approach zero at larger wavelengths. The single scatter albedo, ω, is defined as the ratio of extinction due to scattering to the total extinction,

$$\omega = \frac{\beta_s}{\beta_e}$$

and typically ranges from 0 (no scattering) to 1 (only scattering). Stratus clouds, as well as sulfates, are purely scattering in the visible, while soot is a strong absorber throughout the entire spectrum (middle panel of Fig. 2.1). The bottom panel shows the asymmetry parameter, g, which determines if a particle preferentially scatters radiation in the forwards (> 0) or backwards (< 0) direction, relative to the direction of travel. All three particles scatter in the forward direction, with clouds (soot) scattering radiation forwards most (least) preferentially.

This study focuses on the shortwave part of the spectrum (λ < 4.0 μm), as the diameters of the particles in question are typically on the same order of magnitude as the wavelength, or smaller, thus their interaction falls under either the Mie Scattering Theory or the Rayleigh Regime (Fig. 2.2). Mie Theory for scattering and absorption of spherical particles is essentially broken down into a set of partial differential equations that depend on the index of refraction and size parameter (see Petty, 2006 for further details on Mie Theory). The size parameter relates the particle circumference in μm to the wavelength, also in μm:

$$X = \frac{2\pi r}{\lambda}$$

Using the mode radius from OPAC for each particle, and a wavelength of 1 μm, the size parameters for stratus and sulfates (shown in Fig. 2.2) fall within the Mie Scattering regime, where

$$0.2 < X < 2000.$$

Soot, which is a much smaller particle than the cloud droplets and sulfate particles, falls within the Rayleigh scattering regime in the visible and near infrared. The Rayleigh regime characterizes scattering and absorption by particles that are sufficiently small relative to the wavelength. In Streamer, Rayleigh scattering by air molecules can be turned on or off, and it was included for this study.

2.3 A-Train Validation of Aerosols and Clouds with SEVERI (AVAC-S) Software

The European Organisation for the Exploitation of Meteorological Satellites (EUMETSAT) developed the Spinning Enhanced Visible and InfraRed Imager (SEVERI) to observe the earth at several spectral channels, thus providing information about clouds, and land and sea surfaces. SEVERI is housed on the Meteosat Second Generation (MSG) geostationary satellite, which covers an area from 65°W to 65°E and 65°N to 65°S. SEVERI operates at 12 spectral channels, one of which is called the High Resolution Visible (HRV) channel. The HRV has a sampling distance of 1 km in the visible spectrum, which is important for obtaining cloud and aerosol properties such as cloud phase, optical thickness, and effective radius. NASA's A-Train constellation also includes satellites that can detect the same cloud properties (i.e. CALIPSO, MODIS, CloudSat). A software program, called A-Train Validation of Aerosols and Clouds with

SEVERI (AVAC-S) was developed by EUMETSAT in order to validate cloud products obtained from A-Train satellites against those from SEVERI.

AVAC-S, programmed in the Interactive Data Language (IDL) uses object-oriented programming to match A-Train overpasses with SEVERI observations. The A-Train validation includes data from the following instruments:

- Cloud Profiling Radar (CPR, aboard CloudSat)
- Cloud-Aerosol Lidar with Orthogonal Polarization (CALIOP, aboard CALIPSO)
- Advanced Microwave Scanning Radiometer – Earth Observing System (AMSR-E, aboard Aqua)
- Moderate Resolution Imaging Spectroradiometer (MODIS, aboard Aqua and Terra)

The software maps the A-Train data and the SEVERI data on a common grid, and the combined datasets are stored as Hierarchical Data Format (HDF5) files. For this study, AVAC-S is used to obtain merged datasets for low, liquid water clouds in the South Atlantic Ocean. The criteria used to obtain the merged files are shown in Table 2.2. Only profiles in the area of interest (see Fig. 1.2) that have a Cloud Top Temperature (CTT) larger than 273 K, a positive reference r_e, and Cloud Top Heights (CTH) that fall between 0.3 and 2.5 km are kept. The study includes all A-Train overpasses meeting the above criteria from August 2006 to December 2010.

2.4 Optimal Estimation

One of the most common problems in passive remote sensing is called the "inverse problem" where, given a set of radiances observed by a satellite sensor, we want to obtain a useful estimate of an environmental parameter (e.g. optical depth or effective radius). This involves an estimate whose uncertainty is smaller than the *a priori* uncertainty of the variable (e.g. Petty, 1999). A linear algorithm is used to minimize the variance between the measured value and the true value as explained in Petty (1999) and

Raschke (1996). The optimal estimation method assumes that the errors in the measurements and *a priori* parameters can be described with a Gaussian distribution (Poulsen et al., 2012). A solution is then found by minimizing the cost function, which is the sum of the Gaussian exponents.

Streamer is used to create a lookup table (LUT) of optical depth and effective radius using reflectances at 0.86 and 2.1 μm (see Fig. 4.1). After Streamer is run for each experiment including aerosols, the 0.86 and 2.1 μm reflectances are compared to the reflectances on the LUT using the following equation:

$$x^2 = \frac{(r_{0.86} - LUT_{0.86})^2}{\mu_{0.86}} + \frac{(r_{2.1} - LUT_{2.1})^2}{\mu_{2.1}}$$

where $LUT_{0.86}$ and $LUT_{2.1}$ are all reflectance values in the LUT at those specific wavelengths, and $\mu_{0.86}$ and $\mu_{2.1}$ are the assumed errors at those respective wavelengths. Where x^2 is a minimum, the first guesses for optical depth, τ', and effective radius, r_e', are taken to be those values closest to the nearest τ and r_e pair on the LUT.

Newton's iterative method is then used to fit the LUT reflectances with a non-linear model. The first guesses, τ' and r_e', are used to calculate a Jacobian matrix as defined in Rodgers (2000). A forward model updates the value of the state vector until the Chi-squared error value converges to a minimum (see Rodgers, 2000 for more detailed methodology). Once the error has converged to a minimum value, the updated values of τ' and r_e' are returned.

2.5 Tables and Figures

Temperature Profile	Degrees Latitude	Months
Tropical	30°S to 30°N	All
Midlatitude Summer	30°N to 50°N 30°S to 50°S	April-September October-March
Midlatitude Winter	30°N to 50°N 30°S to 50°S	October-March April-September
Subarctic Summer	50°N to 70°N 50°S to 70°S	April-September October-March
Subarctic Winter	50°N to 70°N 50°S to 70°S	October-March April-September
Arctic Summer	70°N to 90°N 70°S to 90°S	April-September October-March
Arctic Winter	70°N to 90°N 70°S to 90°S	October-March April-September

Table 2.1: Streamer temperature profiles as determined by latitude and month.

Satellite	Sensor	Product	Threshold
Aqua	MODIS	Cloud Top Temp	> 273 K
Aqua	MODIS	Reference Cloud Effective Radius	> 0
CloudSat	CPR	Cloud Top Height	> 300 m
CALIPSO	CALIOP	Cloud Top Height	< 2500 m
-	-	Latitude	30°S < Lat < 5°S
-	-	Longitude	10°W < Lon < 15°E
-	-	Land Sea Mask	= 0 (ocean)

Table 2.2: The thresholds used for several satellite products in order to obtain data for low, liquid water clouds in the area of interest. The latitude, longitude, and land sea mask are generic properties obtained from the A-Train constellation.

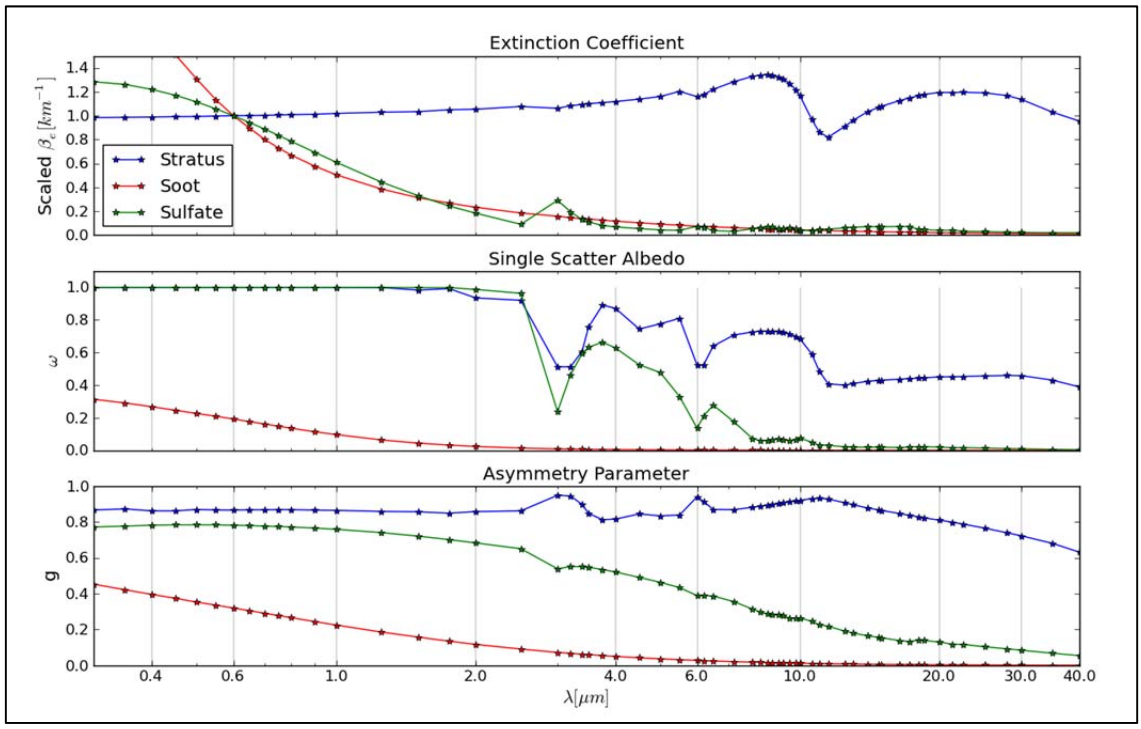

Figure 2.1: Spectral optical properties for maritime stratus clouds (blue), soot (red), and sulfates at 80% relative humidity (green) from the OPAC dataset. (Top) Volume extinction coefficient [km^{-1}] scaled to be 1.0 km^{-1} at 0.6 μm, (middle) single scatter albedo, and (bottom) asymmetry parameter.

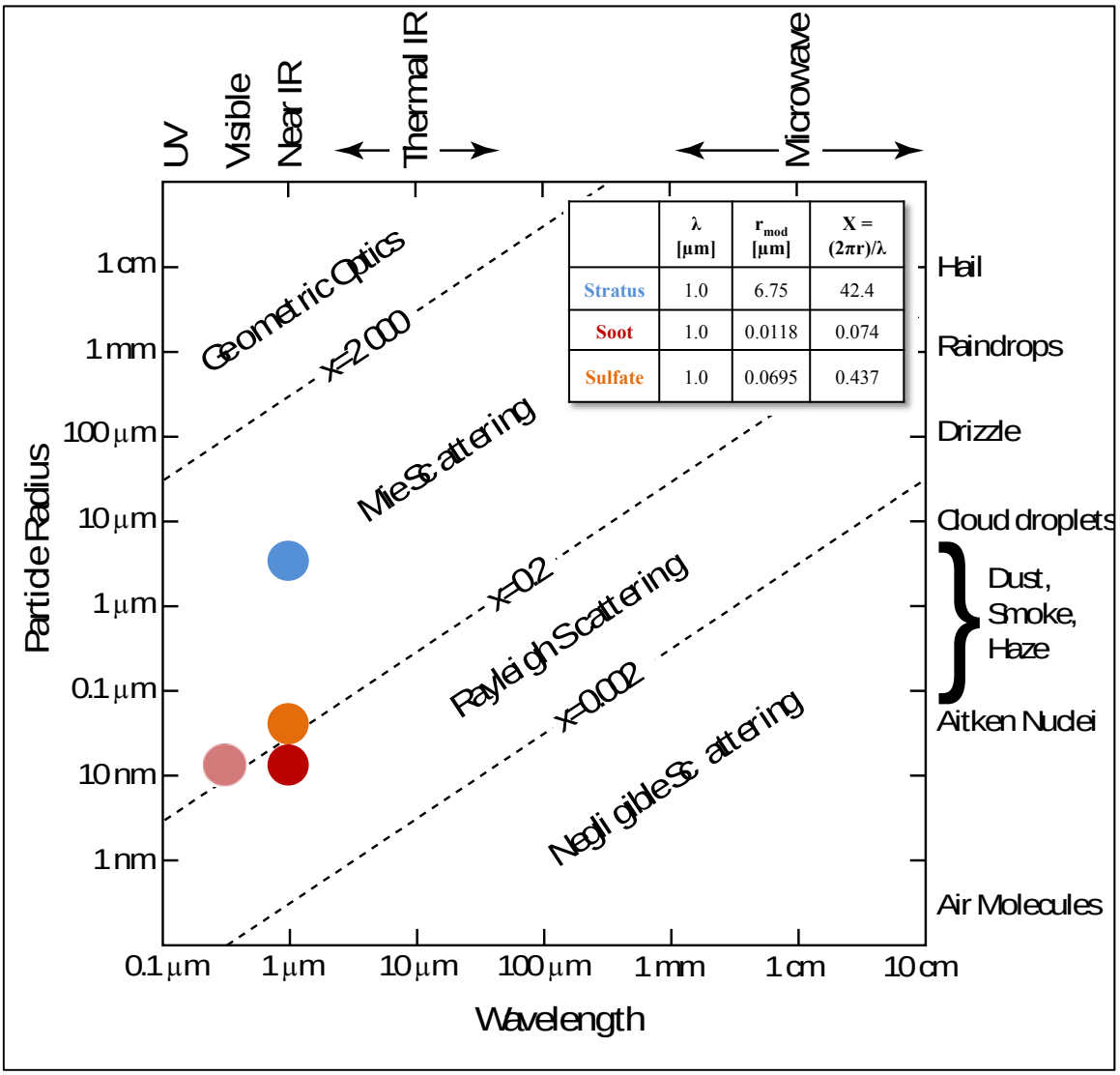

Figure 2.2: Relationship between particle radius, wavelength, and scattering regime. Choosing mode values of particle radii for stratus cloud (blue), and sulfates (orange), both fall within the Mie Scattering regime in the visible and near infrared. Soot falls within the Mie scattering regime at wavelengths below 0.35 µm (light red), and the Rayleigh scattering regime in the visible and near infrared (dark red). *(Adapted from Fig. 12.1 in Petty, 2006)*.

3. Radiative Transfer Sensitivity Studies

Several sensitivity studies are performed in Streamer in order to investigate potential sources of error in our methods. First, the height of the aerosol layer in Streamer is varied from 2 to 4 km, based on a priori observational studies. Next, the number of shortwave and longwave streams used in the radiative transfer calculations is increased. The more streams used, the more accurate the results, but the more computationally time-consuming they become. Finally, Streamer is run with each of the different temperature profiles and the effects on the reflectances are shown. Due to the results of these sensitivity studies, the following experiments are designed to find a balance between resulting errors and computational time.

3.1 Aerosol Layer Height

Previous studies have shown that aerosol layers typically reside between 2-4 km in the region off the coast of Angola and Namibia (Devasthale & Thomas, 2011; Wilcox, 2010). The height of the aerosol layer is varied between 2 and 4 km in Streamer in order to verify that the radiative transfer calculations would be unaffected by the placement of the aerosol layer. A marine stratus cloud base is placed at the surface, with a r_e of 4.0 μm and a τ of 10. The spectral optical properties are taken from the OPAC database (see Section 2.2). An aerosol layer consisting of either soot or sulfates (the optical properties of which are also taken from OPAC) is placed above the cloud, and the shortwave reflectances are then plotted for each band. The aerosol optical depth is set to 0.5. The simulation is run in a tropical atmosphere at 20°N and 0°E with a solar zenith angle of 20.0°.

Figure 3.1 shows the reflectances from each run, and the differences between them. The two Streamer channels used to create lookup tables in the remainder of this study, 0.86 μm and 2.1 μm, are shown as the vertical dashed lines in Figure 3.1. When the base of the aerosol layer is at 2 km, the reflectances are significantly larger by up to 0.2 for soot and 0.6 for sulfates. This is likely due to an overlap of the aerosol layers with the cloud in Streamer. As the aerosol height is increased to 3 and 4 km, the reflectances decrease and there is no change between these two heights for either soot or sulfates (Figure 3.1c and d show zero difference between the 3 and 4 km runs). As an extreme case, the aerosol is placed at 15 km and the reflectances remain the same as they were at 3 km. The experiments performed in this study thus place the aerosol at 15 km in order to avoid any overlap with a potentially thick cloud.

3.2 Number of Streams

Radiative transfer calculations often represent electromagnetic waves by a number of discrete directions, called "streams". The two-stream approximation and its cousin, the Eddington-approximation, are the most common examples. The two-stream approximation assumes that the intensity is constant within either region, while the Eddington-approximation assumes the intensity in each stream follows a linear function of cosine of the zenith angle. A common way to obtain more accuracy in radiative transfer calculations involves using a discrete ordinance method, in which an arbitrary number of "streams" in each hemisphere represent a different direction (Petty, 2006). The larger number of streams identified, the more directions that are represented.

In Streamer, the number of streams for longwave and shortwave calculations can range from 4 to 48, using even numbers only. However, the greater the number of

streams, the more computationally time-consuming the calculations become. The lookup tables produced for this study require 1,880 Streamer runs for all combinations of cloud optical depths and effective radii. The number of streams is increased from 4 to 14 streams, and the reflectances are compared for the two channels of interest to this study (Figure 3.2). As the number of streams increases, the reflectances at 0.86 μm and 2.1 μm remain relatively constant. Table 3.1 shows the time it takes to run one Streamer simulation (at both wavelengths) for one cloud τ and r_e pair. The time it would take to run 1,880 simulations for all τ and r_e pairs is shown in minutes. Both 6 and 8 streams have the least amount of computational time with 3.45 minutes to create a lookup table. We thus chose to use 8 streams for the remainder of this study, as it is slightly more accurate than 6 streams, and still time-efficient.

3.3 Atmospheric Temperature Profiles

Streamer has seven built-in atmospheric profiles (see Table 2.1) with varying temperature, pressure, water vapor density, and ozone density profiles (Ellingson et al., 1991). The Arctic profiles were created using Arctic Ocean station data (Key & Schweiger, 1998). Figure 3.3 shows how each profile varies with height. A Tropical atmosphere, which would be characteristic of the South Atlantic Ocean off the west coast of Africa, shows a very warm surface temperature, and a cold, high tropopause. The troposphere is characterized by high amounts of water vapor and a moderate amount of ozone, when compared to other profiles. Both 0.86 μm and 2.10 μm are affected by water (more strongly at 2.1 μm), thus we expect the reflectances to vary depending on the atmospheric profile used.

Figure 3.4 shows how the reflectances of four individual clouds with specified τ and r_e would change based on the atmospheric profile. With all other variables being kept constant, the change in atmospheric profile – including pressure, temperature, water vapor, and ozone – has a significant effect on the reflectances at both wavelengths. As the profiles transition from tropical to arctic winter, the reflectances at 2.1 μm and 0.86 μm increase. This is likely due to the decrease in water vapor density throughout the atmospheric column closer to the poles. The 2.1 μm band is strongly water absorbing, thus less water vapor in the atmosphere suggests less liquid water in the cloud. This will decrease the absorption at 2.1 μm from the liquid water, thus increasing the transmission of radiation to the top of the atmosphere. The 0.86 μm channel is considered a conservative channel for liquid water, meaning that water is still absorbed at this channel, but a negligible amount.

3.4 Tables and Figures

Streams	Time (s)	Total Time (min)
4	0.11	3.45
6	0.20	6.27
8	*0.11*	*3.45*
10	0.12	3.76
12	0.13	4.07
14	0.16	5.01

Table 3.1: The time it took to run Streamer for an individual optical depth and effective radius pair is shown in seconds, and the time it would take to run 1,880 Streamer simulations is shown in minutes for each number of streams.

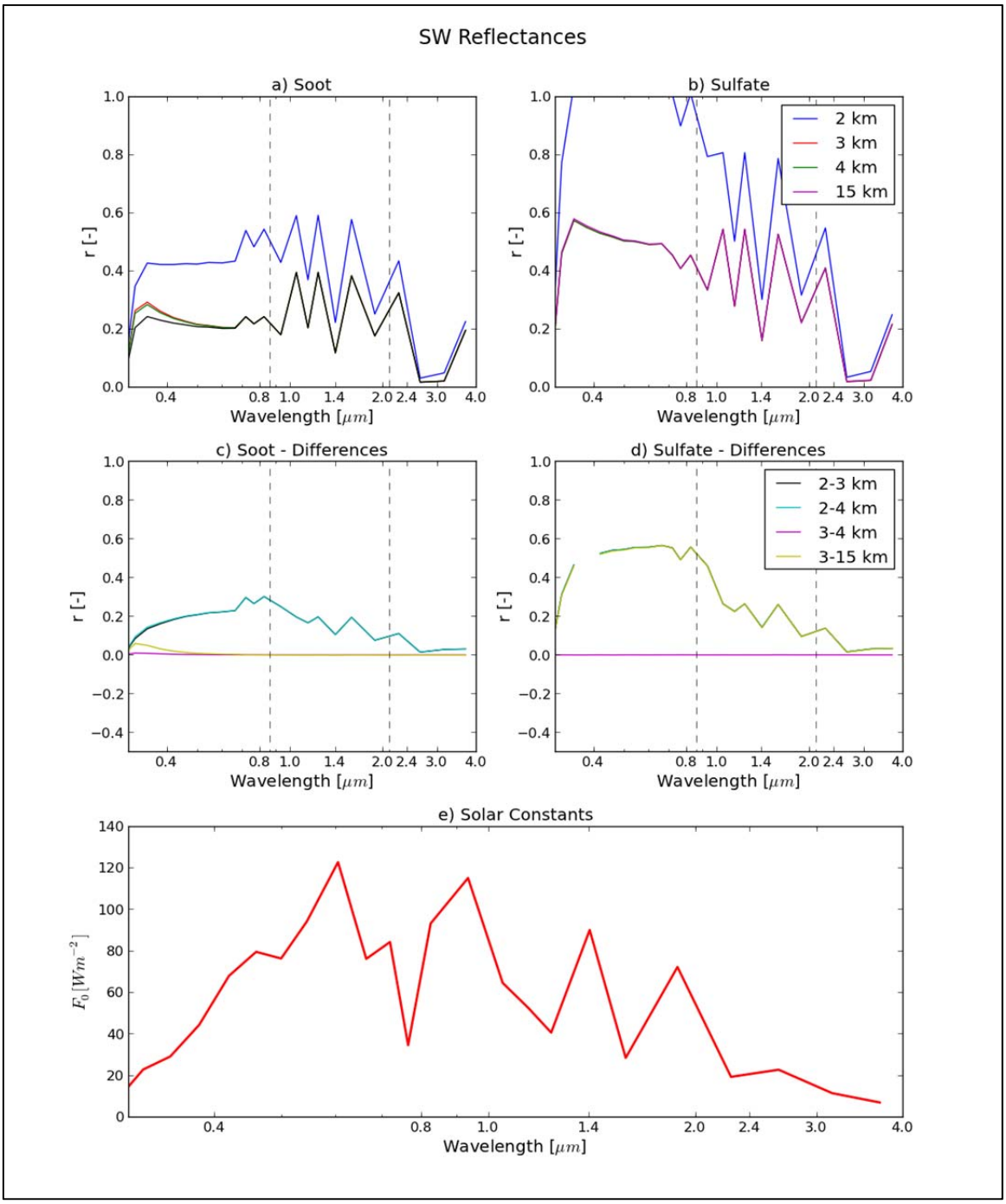

Figure 3.1: Shortwave reflectances for each Streamer run with a cloud base at 0 km and the aerosol layer base at either 2 (blue), 3 (red), 4 (green), or 15 km (magenta). (a) The TOA reflectances with an overlying soot layer. (b) TOA reflectances with an overlying sulfate layer. (c) The differences between the 2 and 3 km runs (black), 2 and 4 km runs (teal), 3 and 4 km runs (magenta), and 3 and 15 km runs (yellow) are shown for soot (d) and sulfates. The vertical dashed lines represent 0.86 and 2.10 µm, the two Streamer channels of interest to this study. e) The solar constants in W m^{-2} used for each band in Streamer.

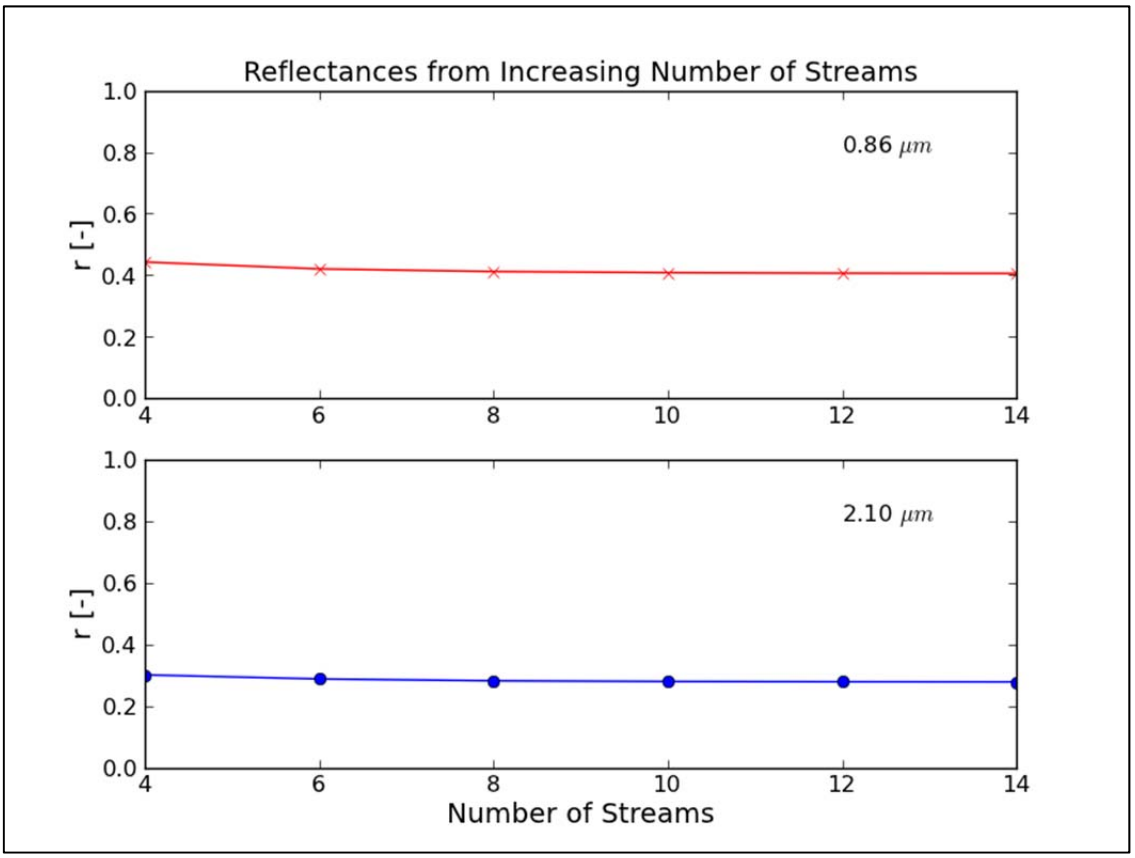

Figure 3.2: The number of Streams used in Streamer calculations is increased from 4 to 14 and the resulting TOA reflectances at 0.86 μm (top, red) and 2.10 μm (bottom, blue) are shown.

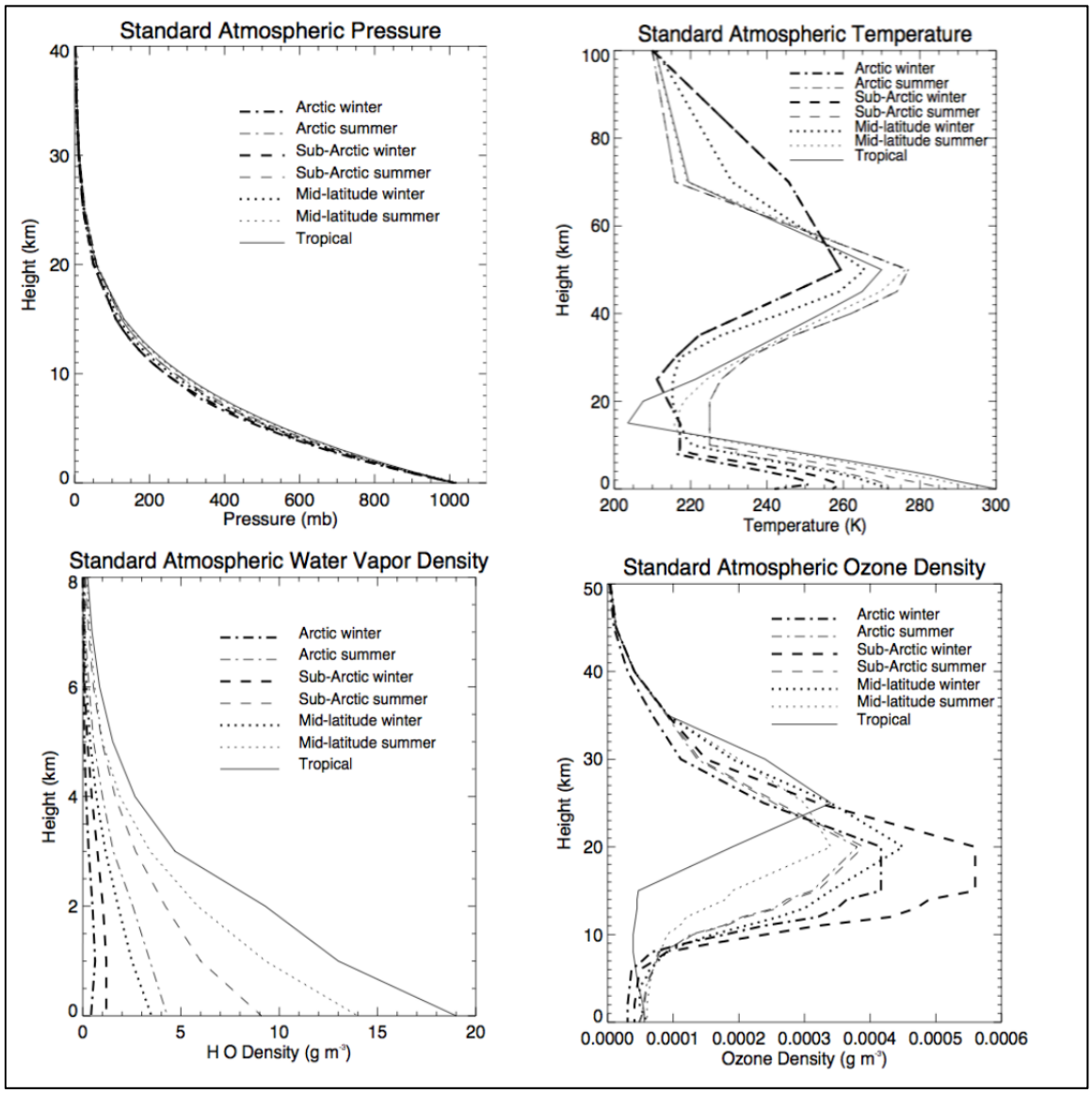

Figure 3.3: Streamer built-in atmospheric profiles with varying pressure (top left), temperature (top right), water vapor density (bottom left), and ozone density (bottom right). All profiles, except the Arctic profiles, are from (Ellingson et al., 1991). Arctic profiles are determined from Arctic Ocean station data (Key & Schweiger, 1998). *Figure adapted from Key & Schweiger, (1998).*

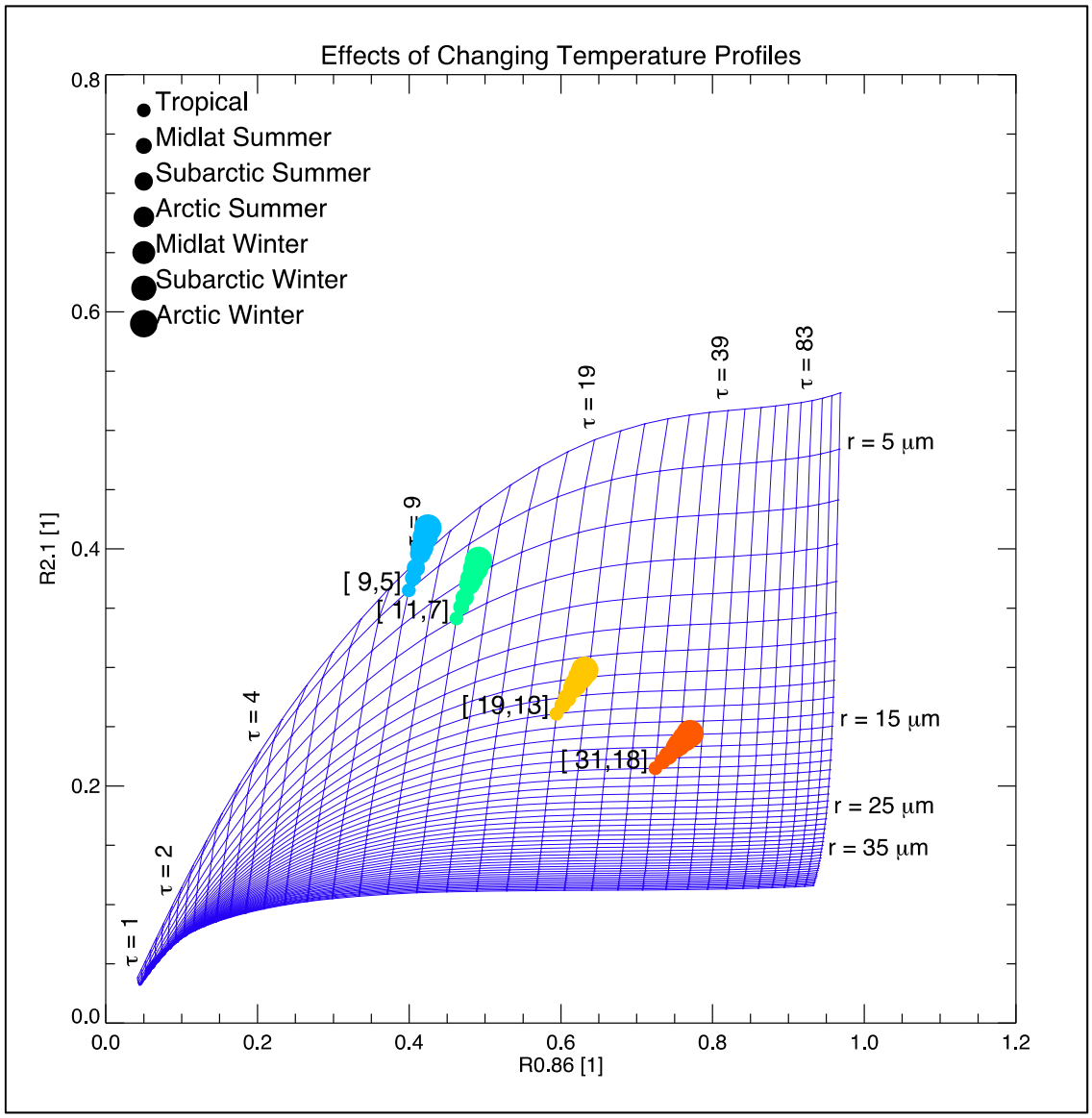

Figure 3.4: For four different clouds [τ, r_e], the atmospheric profile is changed from Tropical to Arctic winter and the resulting reflectances are plotted over a lookup table (tropical).

4. Simulated Retrievals

Several studies have investigated the effects of biomass burning aerosols on MODIS retrievals of underlying cloud optical properties (Cattani et al., 2006; Haywood et al., 2004; Meyer et al., 2013). MODIS relies on reflectance measurements in the visible and near infrared to retrieve cloud optical thickness and effective radius, and the neglect of aerosols above the cloud can lead to systematic biases in the retrievals. This section outlines the results from radiative transfer model experiments that calculate reflectances from stratus clouds and overlying aerosol layers. Optimal estimation (see Section 2.4) is then used to estimate the impact on cloud retrievals.

4.1 Cloud Reflectances and Impact of Overlying Aerosols

Several simulations are run in Streamer and the reflectances at 0.86 μm and 2.1 μm are calculated (see Section 2.1). A water-absorbing band (2.1 μm) and a water non-absorbing band (0.86 μm) are used in order to retrieve τ and r_e. The 0.86 μm channel is used, as opposed to the 0.6 μm channel, in order to minimize the reflectance from the surface ocean and Rayleigh scattering in the atmosphere (Platnick et al., 2003). The retrieved r_e from MODIS is shown to be more accurate at 2.1 μm than at 1.6 μm, regardless of the overlying aerosol layer when comparing radiative transfer simulations to MODIS observations (Cattani et al., 2006). For each Streamer run, 8 shortwave and 8 longwave streams are used with 16 phase function Legendre coefficients. Radiances are calculated, including gaseous absorption and Rayleigh scattering, at 20°N and 0°E. The surface is 100% open ocean water, and the surface albedo is determined by the Streamer internal database. Scaling the background optical depth to zero turns off all background tropospheric aerosols.

First, a maritime stratus cloud is modeled with varying combinations of τ and r_e, and the reflectances are compiled into a LUT with the vertical lines representing τ increasing to the right, and the horizontal lines representing r_e increasing to the bottom (Figure 4.1). Different LUTs are used to obtain τ and r_e for different cloud types and different scenes (over ocean or land, i.e.). Four experiments are performed where a layer of soot is placed above a maritime stratus cloud with specified τ and r_e, using the spectral optical properties from OPAC (Section 2.2). The cloud is placed between 0-1 km and the base of the aerosol is set to 3.5 km. The aerosol optical depth (AOD) is then increased from 0 to 1 in increments of 0.1 and the resulting reflectances are plotted on top of the LUT (Figure 4.2). For each case, as the soot optical depth increases, the reflectances at both wavelengths decrease dramatically.

The same four experiments are performed for a layer of sulfates at 80% relative humidity above four clouds with the same specified τ and r_e. Figure 4.3 shows a much smaller effect on the reflectances at both wavelengths. For the first two clouds (blue and green), the reflectances at 0.86 μm slightly increase, while the reflectances at 2.1 μm barely change. The third cloud (orange) exhibits almost no change in either the 0.86 μm or 2.1 μm reflectances. The fourth cloud (red) shows a slight decrease in 0.86 μm reflectances, and a very slight decrease in 2.1 μm reflectances.

The change in reflectances is seen more clearly in Figure 4.4. The most dramatic difference occurs for soot aerosols at 0.86 μm, where the reflectances decrease dramatically with a larger AOD. At both wavelengths, sulfate aerosols show little effect on the reflectances. This is likely due to the difference in single scatter albedo between soot and sulfates (see Fig. 2.1). Soot is much more strongly absorbing than sulfates,

which are purely scattering aerosols in the forward direction. The soot aerosols are more likely to absorb the incoming solar radiation as well as any reflected solar radiation from the cloud below, therefore decreasing the radiation that reaches the top of the atmosphere.

4.2 Impact on Cloud Retrievals

It has been shown that absorbing aerosols that lie above a liquid water cloud can lead to an underestimation in the retrieved cloud optical depth and effective radius from satellites (Cattani et al., 2006; Haywood et al., 2004; Meyer et al., 2013). These studies use a combination of observations and radiative transfer models to show how an absorbing aerosol layer of a specific AOD affects the MODIS retrievals. This study uses a similar theoretical approach to determine the change in reflectances due to overlying aerosols of varying optical thicknesses. Optimal estimation is used to convert the reflectances at 0.86 μm and 2.1 μm to a retrieved cloud optical depth and effective radius, τ' and r_e', respectively.

For each of the four clouds discussed in Section 4.1, the reflectances are converted into a retrieved τ' and r_e' and compared to the original values. Figure 4.5 shows how τ' and r_e' are affected by increasing AOD. For each case, as the soot AOD increases, τ' becomes severely underestimated. This is especially true for the thickest cloud (τ = 31.1, r_e = 18.0 μm): when the AOD is 1.0, τ' = 5.0, which is 16.1% of the actual optical depth. Sulfates, however, have a varying effect: for small τ, the retrieved τ' becomes slightly overestimated with increasing AOD. As τ increases, the effect flips, and τ' becomes slightly underestimated with increasing AOD.

Combinations of reflectances at different channels are used to retrieve r_e, and the MODIS 0.86/1.63 μm combination has been shown to produce a lower bias in r_e than

other channel combinations (Meyer et al., 2013). This effect is not due to the presence of the aerosols, directly, but due to the perpetuation of the reflectance bias throughout the MODIS algorithms. A decision tree is used to determine the phase of the cloud in which the 2.1 or 1.6 μm reflectances are used in combination with the 0.67 μm (Platnick et al., 2003). Once the cloud phase is determined, the effective radius is calculated using a LUT specific to that cloud type. Having previously shown that there can be a significant bias in both the 2.1 μm and 1.6 μm reflectances when aerosols are included, we would expect this bias to affect the r_e retrievals as well.

Figure 4.5 shows the effect of increasing AOD on r_e' for the four cloud experiments. The experiments with sulfates show slight overestimations in r_e' with increasing AOD. Figure 4.2 shows that the first two clouds can display reflectances that no longer lie on the LUT as the soot AOD is increased. This translates into a failed retrieval, and negative r_e' values from optimal estimation methods. For the last two clouds, r_e' is initially overestimated with increasing soot AOD, and eventually underestimated for larger AOD. An interesting effect occurs with r_e' when absorbing aerosols are included: at smaller AODs, r_e' is overestimated. We can see this in Figure 4.2 when the last two clouds (yellow and orange) start to dip towards higher values of r_e with increasing AOD. At some AOD, the effect switches, and r_e' becomes underestimated. This is harder to see in Figure 4.2 as the grid gets more compact at lower reflectances.

Another way to view the optimal estimation retrievals is through a percent change, where τ' and r_e' are compared to τ and r_e via the following relationships:

$$\Delta\tau = \frac{\tau - \tau'}{\tau}$$

$$\Delta r_e = \frac{r_e - r_e'}{r_e}$$

An overestimation of the OE retrievals will manifest itself as a negative percent change, and vice versa. Figure 4.6 shows that retrievals of soot optical depth and soot effective radius exhibit very large percent changes from their true values. As the AOD increases, $\Delta\tau$ increases by up to 60-80%, suggesting that thicker aerosol layers result in a very large underestimation in τ'. For sulfates, $\Delta\tau$ can be over- or underestimated depending on the cloud. The magnitude of $\Delta\tau$ for sulfates, however, is significantly smaller than that of soot. The same is true for Δr_e, with sulfates causing a slight overestimation of effective radius, and soot experiencing a much larger magnitude percent change. The first two clouds exhibit odd behavior in Figure 4.6, as OE methods retrieved negative r_e' values at certain AODs. The magnitude and sign of Δr_e changes with increasing AOD from negative (overestimation) to positive (underestimation).

If an absorbing aerosol lies over an optically thin cloud with small effective radii, the reflectances will fall off the LUT, thus biasing the MODIS retrievals to either underestimate cloud optical depth and effective radius or throw out the pixel entirely. For optically thick clouds, an absorbing aerosol has a much more significant effect on τ' and r_e' than a scattering aerosol, leading to a significant underestimation of τ'. When the aerosol layer is optically thick, the magnitude of this underestimation increases. For scattering aerosols, the effect on τ' and r_e' is much smaller. For optically thin clouds, τ' and r_e' are slightly overestimated. For thicker clouds, τ' becomes slightly underestimated, while r_e' remains overestimated. This effect can also be seen in Figure 4.3, where the thicker (thinner) clouds move towards lower (higher) optical depths with increasing AOD. Although previous studies have observed the underestimation in τ' and r_e' (Cattani

et al., 2006; Haywood et al., 2004; Meyer et al., 2013), few have modeled the changing effects on these retrievals with increasing AOD. The varying effects of soot AOD on r_e' and sulfate AOD on τ' can lead to significant biases in studies that utilize these retrieved properties from MODIS.

4.3 Figures

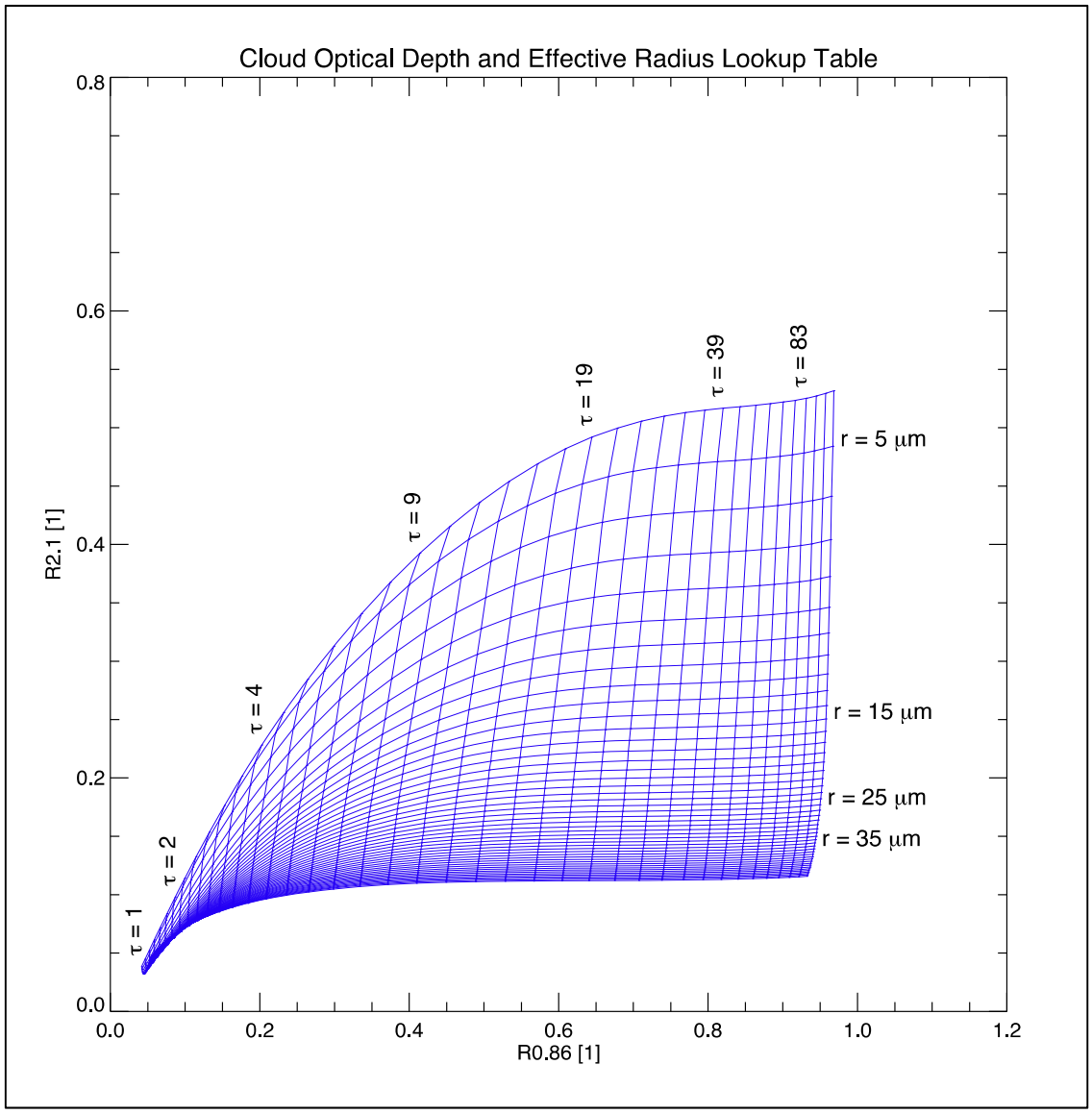

Figure 4.1: LUT generated from Streamer reflectances from several optical depth and effective radius combinations for a maritime stratus cloud.

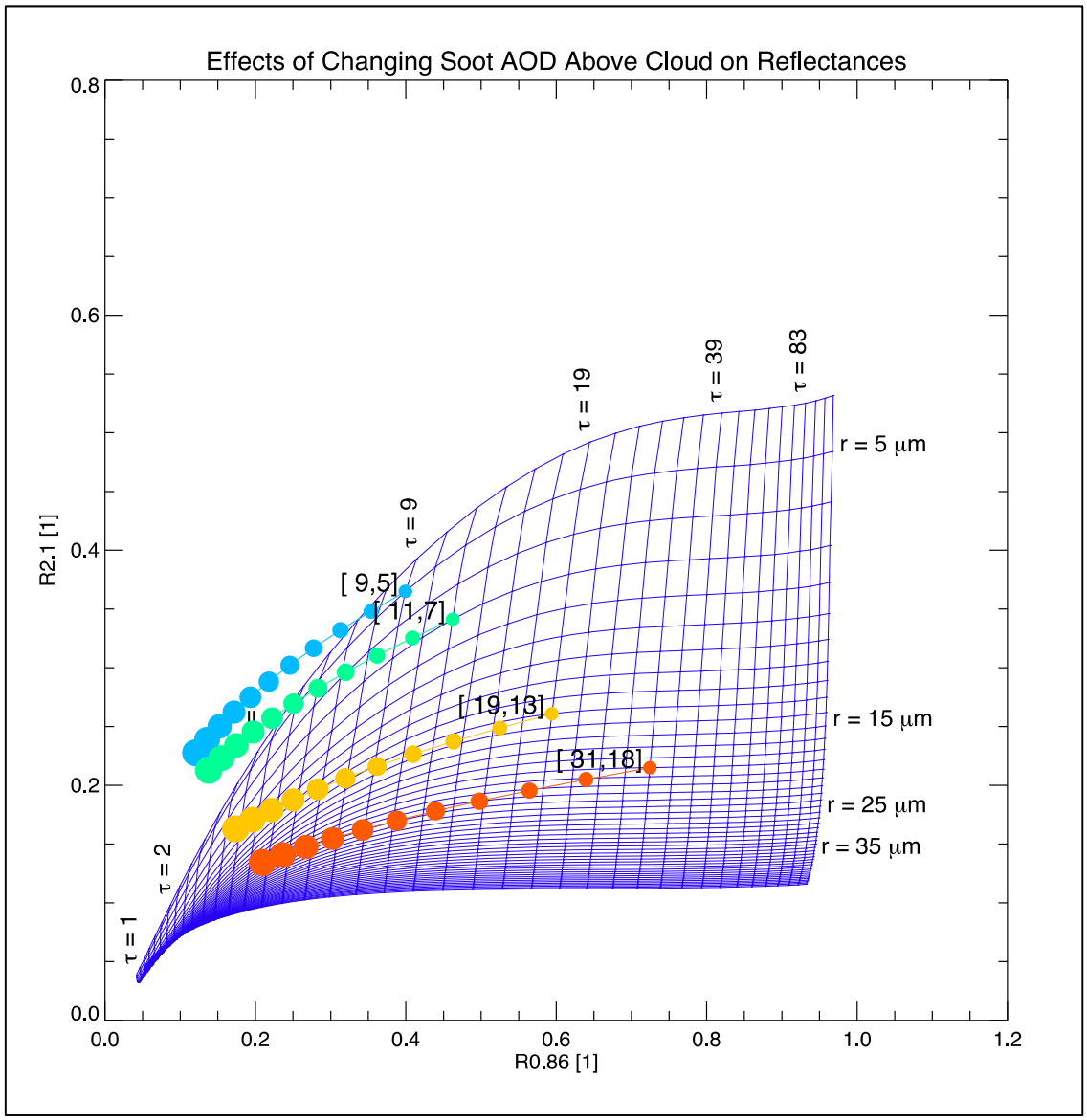

Figure 4.2: Same as Fig. 3.1 with overlying soot experiments. Soot layers are placed at 3.5 km, above four clouds with specified τ and r_e at 0-1 km, shown as [τ, r_e]. Soot AOD increases from 0 (smallest dot) to 1 (largest dot).

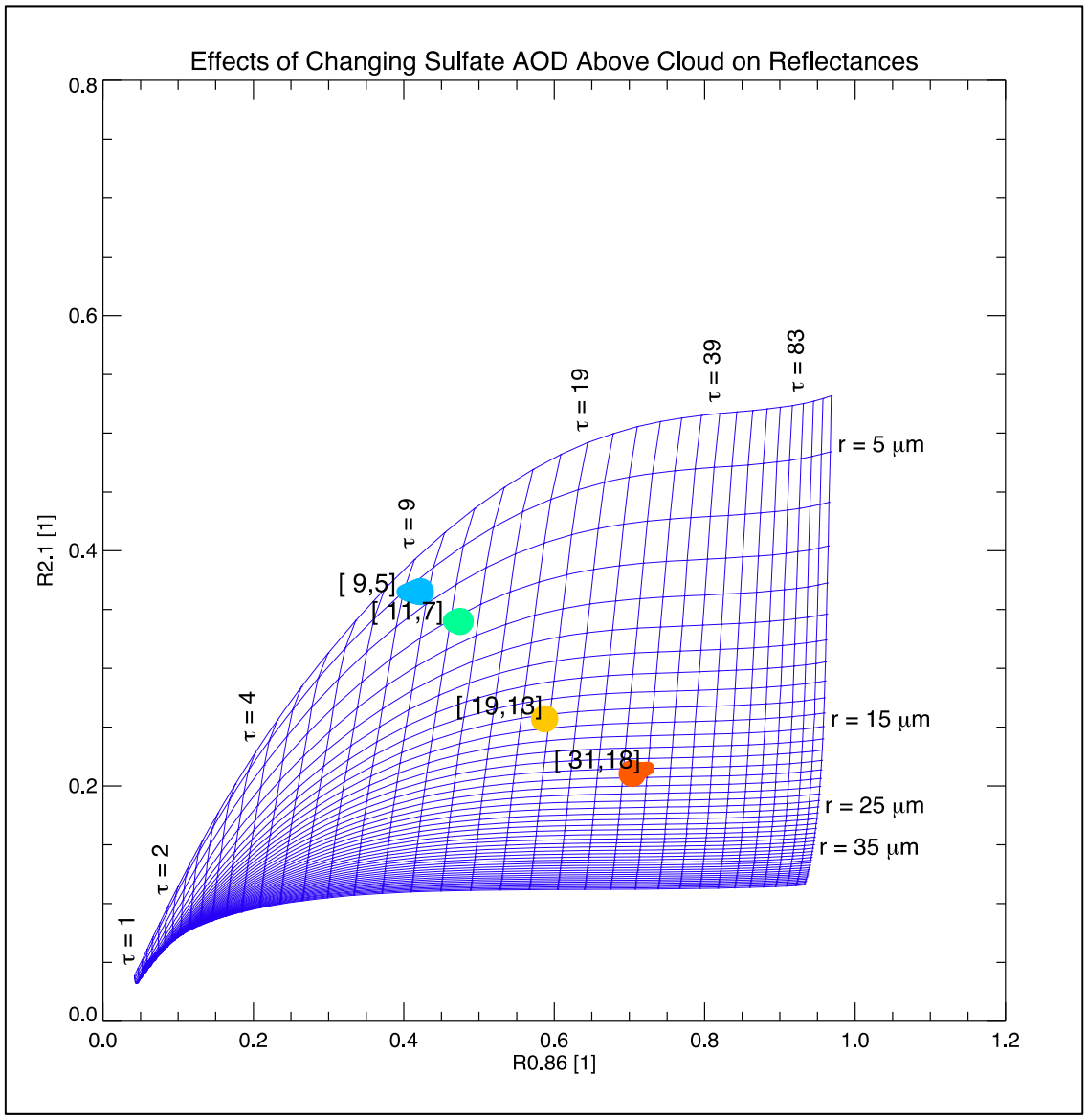

Figure 4.3: Same as Figure 3.2 with sulfates.

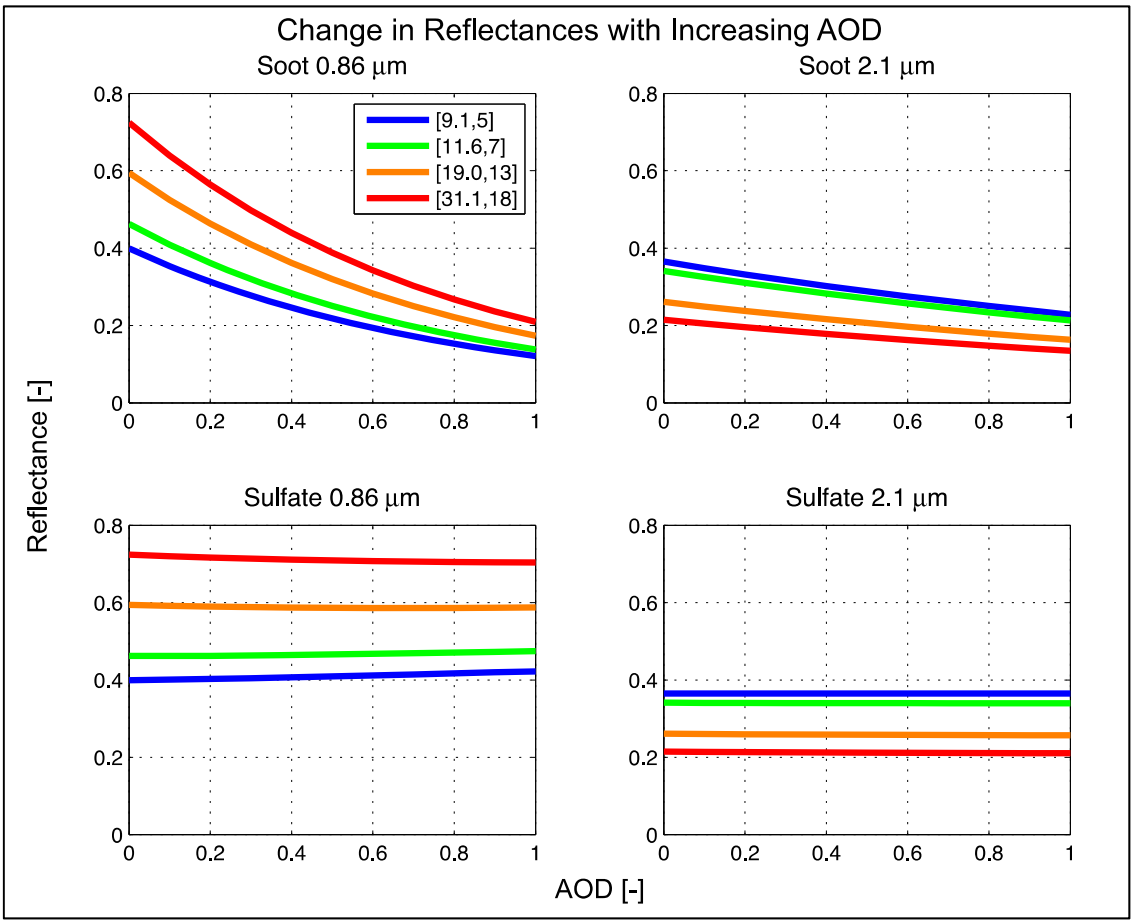

Figure 4.4: The changes in TOA reflectances at 0.86 μm (left column) and 2.1 μm (right column) are plotted against increasing AOD above four clouds with different [τ, r_e]. The top (bottom) row shows experiments with soot (sulfate) aerosols above the cloud.

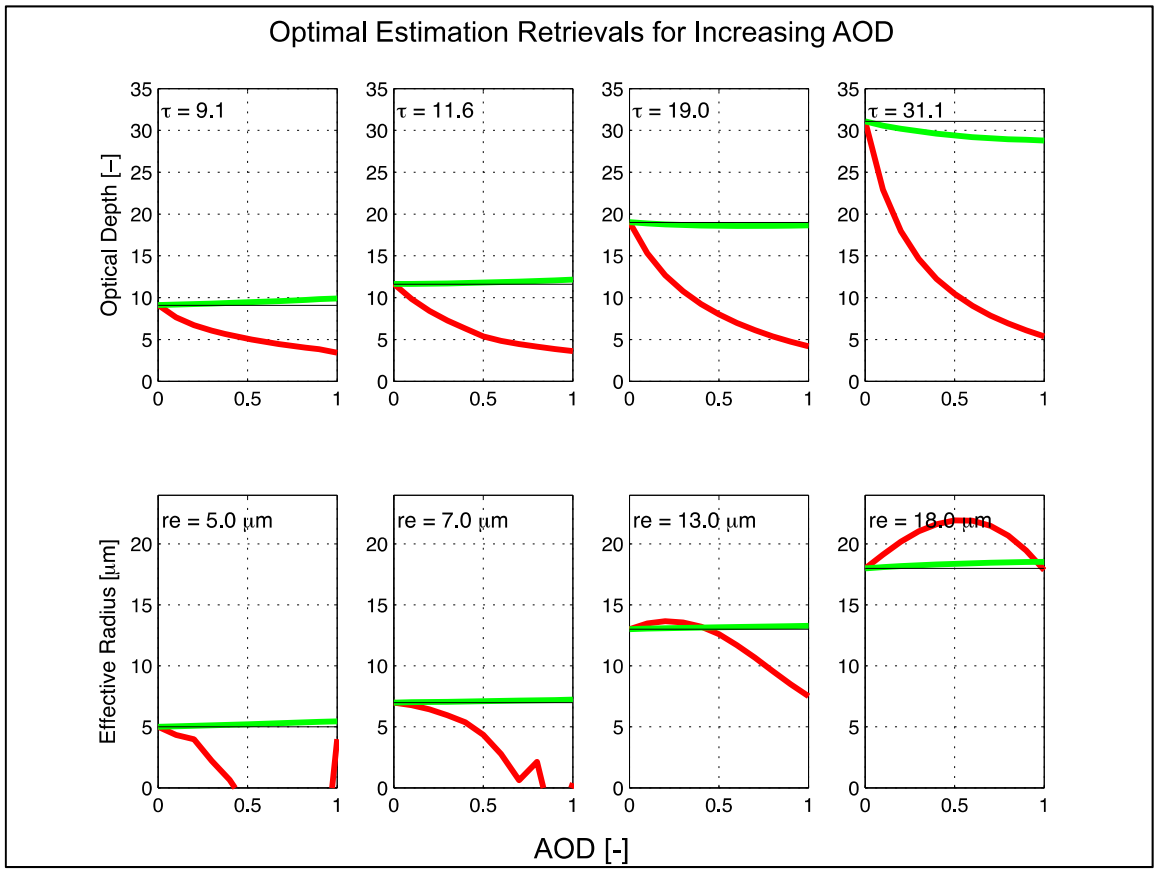

Figure 4.5: For each of the four clouds in Figures 4.2-4.4, optimal estimation shows the effects of increasing soot (red) and sulfate (green) AOD on the retrieved τ' and r_e'. The black lines show the original τ and r_e inputted into Streamer. The original τ and r_e are also written in the top left of each box.

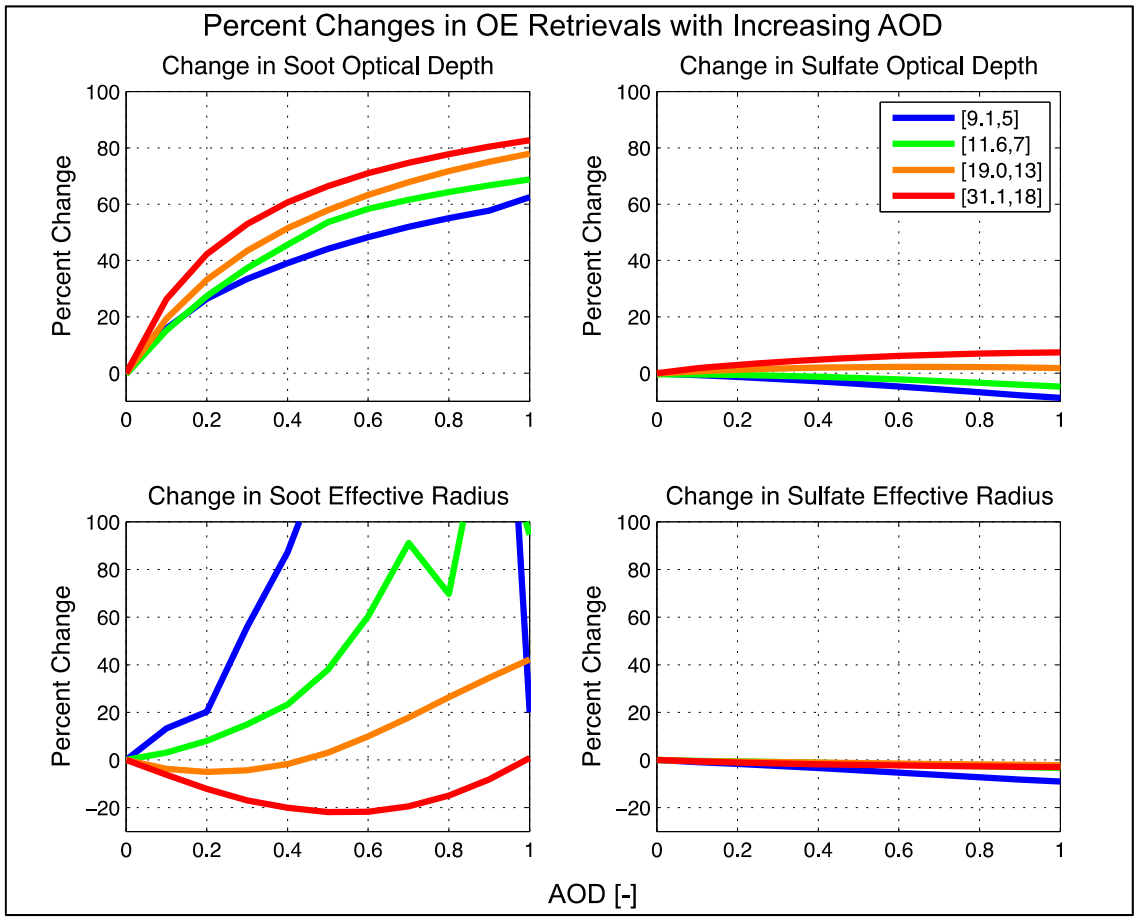

Figure 4.6: Percent change in OE retrievals of soot optical depth (top left), sulfate optical depth (top right), soot effective radius (bottom left), and sulfate effective radius (bottom right) for all four clouds in Figures 4.2-4.5.

5. Satellite Retrievals

Data from the A-Train constellation are taken from August 2006 to December 2010. Vertical profiles are selected based on a set of criteria, selecting only low, liquid water clouds in the region of interest in the South Atlantic Ocean (see Table 2.2). In order to investigate the effects of aerosol layers on cloud properties, the profiles are separated into different bins in which the aerosol layer is touching the cloud or is not touching the cloud. The process to separate the profiles is explained in this section. The effects of the aerosol layers (touching or not) are investigated in this section as well.

5.1 Determining Aerosol Layer Height

This study uses backscatter data from Cloud-Aerosol Lidar with Orthogonal Polarization (CALIOP) (see Section 1.2) to determine whether or not an aerosol layer is vertically separated from the cloud top, or if it is directly interacting with the cloud. CALIOP is an active lidar that measures vertical and horizontally polarized backscatter at 532 nm, and total attenuated backscatter at 1064 nm. The Cloud and Aerosol Layer products calculate aerosol and cloud features based on the 532 nm backscatter ratios (Vaughan et al., 2005). Several studies have used these products to show that aerosol layers are often vertically separated from the cloud, situated between 2 and 4 km in the atmosphere (Devasthale & Thomas, 2011; Wilcox, 2010, 2012). This study uses total attenuated backscatter (TAB) from the 1064 nm channel as it reduces the amount of attenuation that is unavoidable at 532 nm. This allows daytime observations to be included in the dataset. At 532 nm, daytime backscatters are noisy due to the strong scattering of sunlight into the path of the lidar.

In order to sort the vertical profiles into separate bins based on whether or not the aerosol layer is vertically separated from the cloud, several vertical profiles of various parameters are visually investigated. The optical depth is determined by vertically integrating the 1064 nm TAB. A threshold is arbitrarily set for the 1064 nm optical depth values in a 600 m layer above the cloud. The layer extends from 150 m to 750 m above the cloud top. If the difference in optical depths in this 600 m layer is greater than 0.025, the aerosol is assumed to be touching the cloud top. If the difference is less than 0.005, the aerosol is assumed to be vertically separated form the cloud top. Every other value falls under an 'uncertain' bin. Figures 5.1 and 5.2 show two examples of profiles where the aerosol layer is touching the cloud (Fig. 5.1) and not touching the cloud (Fig. 5.2). Panels c and d on both Figures show the changes in optical depth within the 600 m layer: for an aerosol layer that is touching the cloud, the optical depth will dramatically decrease in that layer, whereas it stays relatively constant for the opposite case. The change in optical depth with height also shows a much larger increase within the 600 m layer for the case with the aerosol layer touching the cloud. This increase is not as obvious in Figure 5.2d.

Based on this methodology, each profile from August 2006 – December 2010 is separated into one of three bins: touching, not touching, or uncertain. The number of vertical profiles in each bin is shown by month in Figure 5.3. The months characterized by high biomass burning in Namibia and Angola (JJA and SON) experience large increases in cases where the aerosol layer touches the cloud, while these cases become very uncommon in the off-season (DJF and MAM). The two different cases will have very different effects on the cloud microphysical properties. The cloud droplet number

concentration is calculated for each individual cloud, and the average concentrations are compared for both bins.

5.2 Effect of Aerosols on Cloud Droplet Number Concentration and Effective Radius

The Cloud Droplet Number Concentration (hereby referred to as N) is calculated using Equation 9 in Bennartz (2007)

$$N = \frac{2^{-5/2}}{k}\tau^3\left[\frac{W}{C_F}\right]^{-5/2}\left[\frac{3}{5}\pi Q\right]^{-3}\left[\frac{3}{4\pi\rho_l}\right]^{-2}c_w^{1/2}$$

where liquid water path (W) is described by

$$W = \frac{5}{9}\rho_l \tau r_e$$

which assumes an adiabatically stratified cloud. The ratio between the volume mean radius to r_e, denoted k, is assumed to be a constant 0.8, based on Figure 8 from Lu and Seinfeld (2006). The scattering efficiency, Q, is assumed to be a constant 2.0, which is a typical value for the Mie Scattering Regime (Petty, 2006). The density of liquid water, ρ_l, is 1000 kg m^{-3}. Cloud fraction (C_F), τ, and r_e are taken from MODIS observations. The condensation rate, c_w in g m^{-4}, is calculated using the cloud top temperatures from MODIS. The clouds are assumed to be at 80% of their adiabatic value, so c_w is multiplied by a factor of 0.8 (Bennartz, 2007). N is reported in droplets per cm^3, or simply cm^{-3}.

For both aerosol layers touching the cloud and aerosol layers separated from the cloud, N is compared to a proxy aerosol optical depth. The optical depth at 1064 nm is multiplied by 31, the biomass burning lidar ratio determined by the CALIOP Algorithm Theoretical Basis Document (Liu et al., 2005). In order to correct for lidar noise during the daytime, a constant offset is subtracted. The proxy aerosol optical depth (PAOD) is

taken to be the total optical depth 90 m above the cloud top, determined by vertically integrating CALIOP backscatters.

The clouds are sorted by liquid water path (LWP), as determined by AMSR-E. The results are shown in Figure 5.4. Clouds with smaller (larger) LWPs are associated with smaller (larger) r_e, while the relationship between LWP and N is not as well defined. This suggests that as clouds get thicker (LWP increases), the effective radius increases and N stays more or less constant as predicted by adiabatic theory. N is consistently lower in cases where the aerosol layer is touching the cloud, which is an indication of the first indirect aerosol effect (IAE). The first IAE suggests that an increase in aerosol concentration with in a cloud of constant LWP will increase the number of cloud droplets, N, and decrease the droplet size, r_e.

Surprisingly, when the aerosols are touching the cloud, neither N nor r_e dramatically increase or decrease with increasing PAOD. However, when PAOD increases in aerosol layers that are not touching the cloud, N increases and r_e decreases more dramatically. This effect becomes weaker around PAOD=0.4 (Fig. 5.4b,d) when the N-curves flatten out. This effect is also evident when PAOD < 0.4 in cases where the aerosol layer touches the cloud (Fig. 5.4a,c). The IAE suggests an increase in N and decrease in r_e with increasing PAOD which is evident when PAOD < 0.4. The effect of overlying aerosols on MODIS retrievals is most evident when PAOD > 0.4. When the aerosol is touching the cloud, the trends in N and r_e are likely a combination of the IAE and the bias in the MODIS retrievals.

5.3 Figures

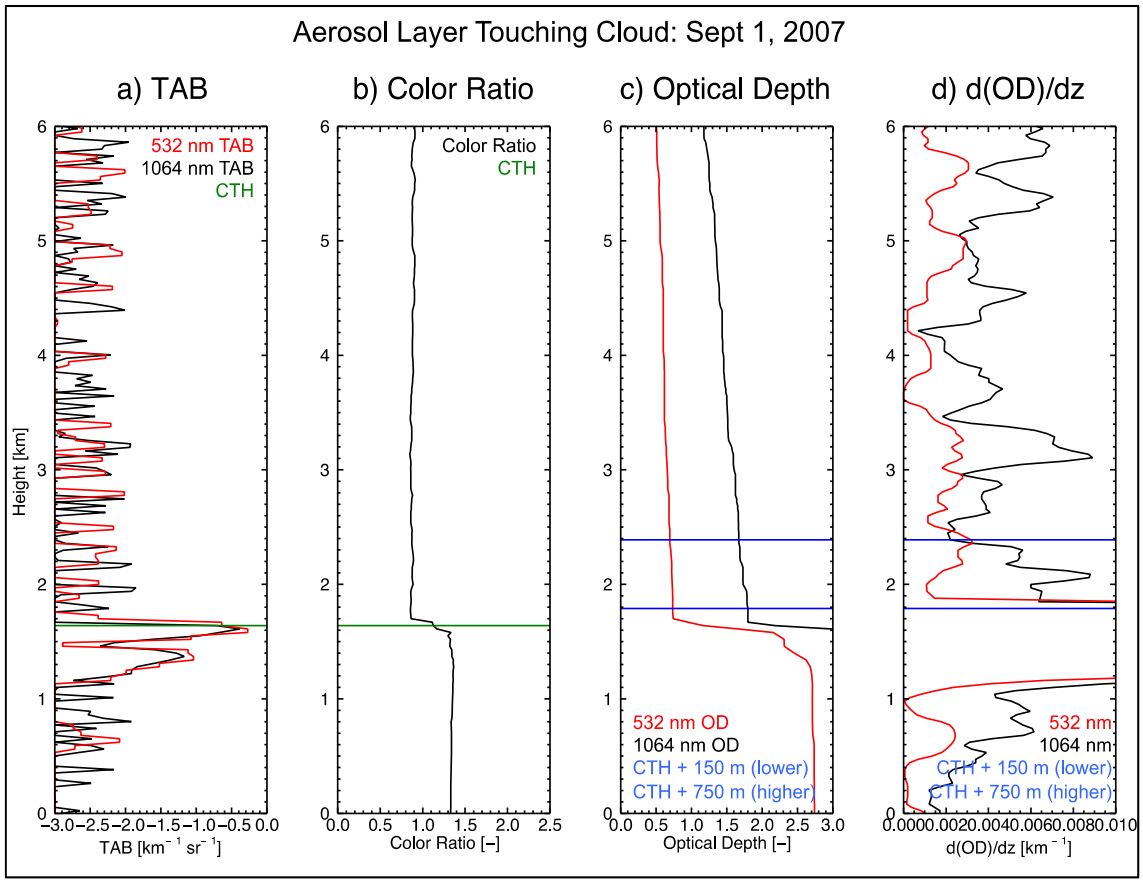

Figure 5.1: Vertical profile from September 1, 2007 showing an aerosol layer touching the cloud, based on our methodology. a) The total attenuated backscatter (TAB) from 532 nm (red) and 1064 nm (black) in [km^{-1} sr^{-1}], b) the color ratio, which is defined as the ratio of vertically-integrated 1064 nm backscatter to the vertically-integrated 532 nm backscatter, c) optical depths from 532 nm (red) and 1064 nm (black) with the 600 m layer outlined by blue lines, and d) the change in optical depth with height for 532 nm (red) and 1064 nm (black). 150 m above the cloud top is the bottom of the 600 m layer, with the cloud top height plus 750 m being the top of the layer.

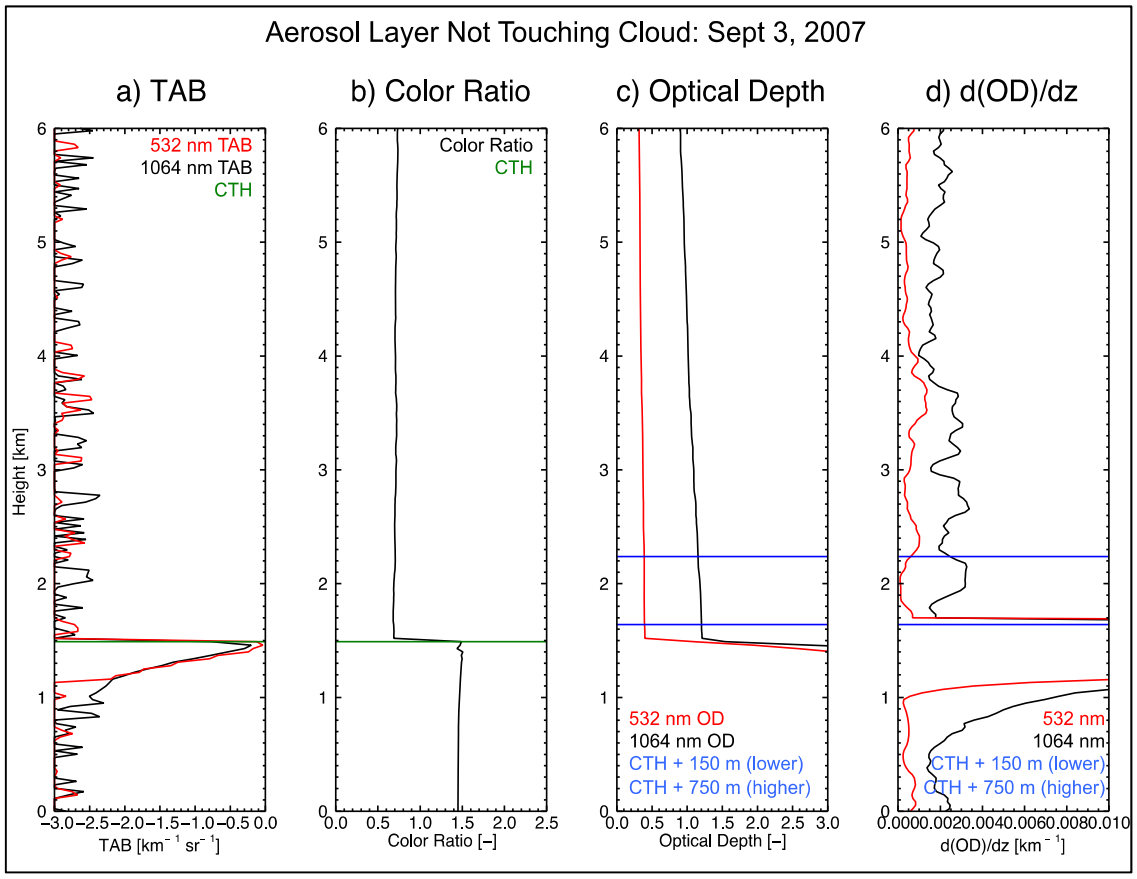

Figure 5.2: Same as Figure 5.1 for an aerosol layer not touching the cloud on September 3, 2007.

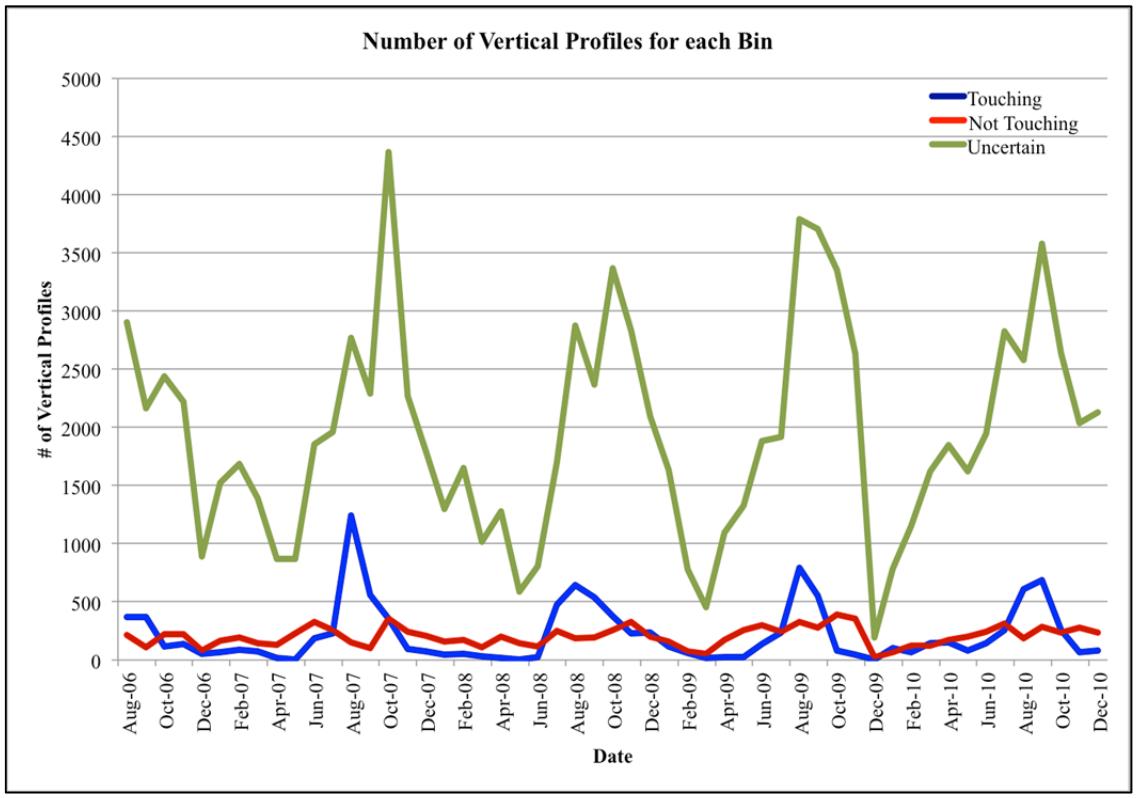

Figure 5.3: The number of vertical profiles by month for aerosol layers touching the cloud (blue), aerosol layers not touching the cloud (red), and the uncertain bin (green).

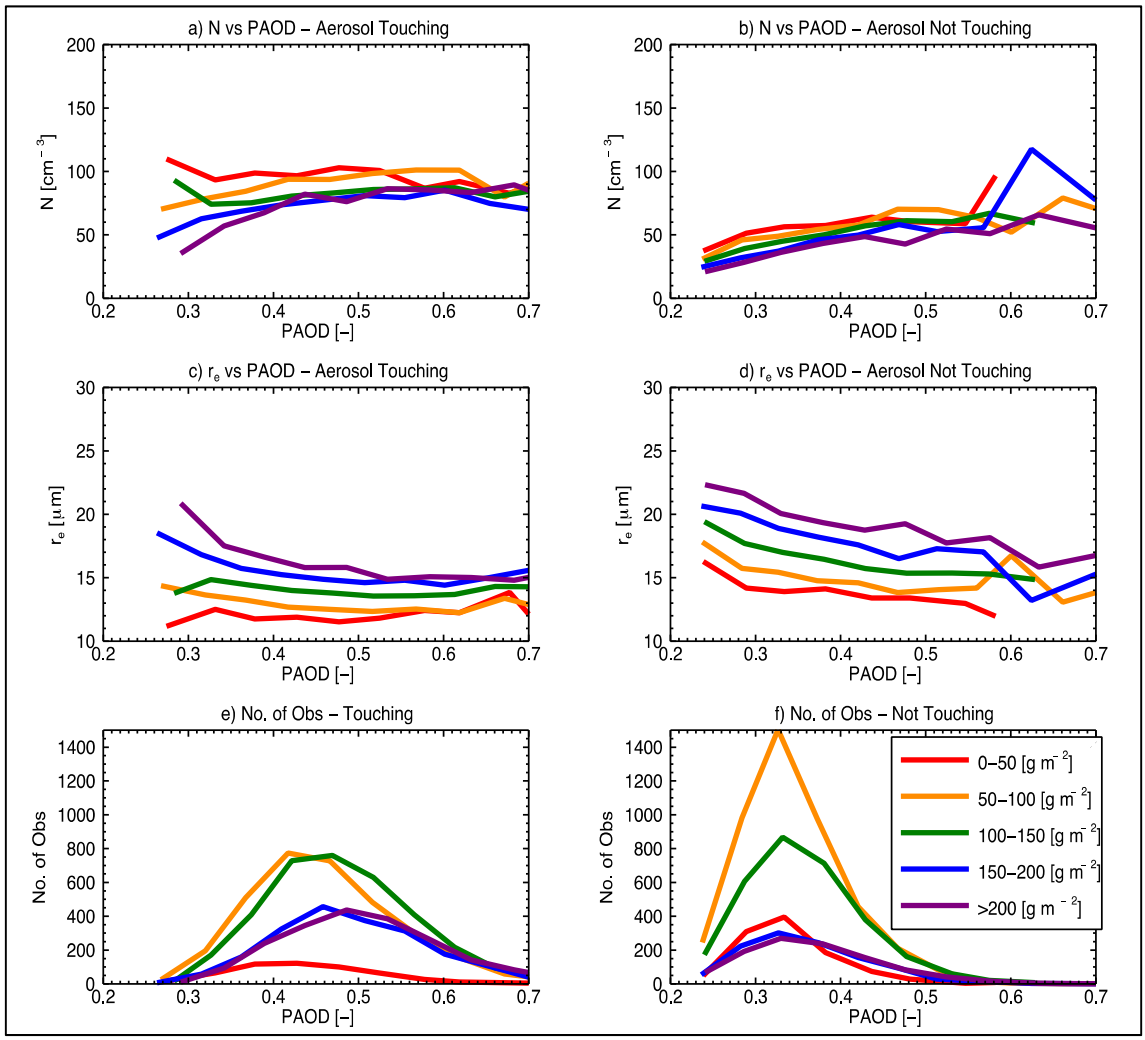

Figure 5.4: For aerosol layers touching the cloud binned by AMSR-E LWP [g m^{-2}], Proxy Aerosol Optical Depth (PAOD) is compared to a) Cloud Droplet Number Concentration (N) in cm^{-3} and c) effective radius (r_e) in μm. The number of observations in each bin is shown in e). For aerosol layers not touching the cloud binned by LWP, PAOD is compared to b) N and d) r_e. f) shows the number of observations in each bin.

6. Conclusions

Previous studies have shown that aerosol layers from biomass burning in the South Atlantic Ocean typically reside between 2 and 4 km in the atmosphere, vertically separated from the prevalent liquid water stratocumulus clouds below (Devasthale & Thomas, 2011; Hobbs, 2002; Wilcox, 2010). Several studies, using satellite measurements as well as radiative transfer models, show that MODIS can severely underestimate cloud optical depth in this region (Cattani et al., 2006; Haywood et al., 2004; Meyer et al., 2013). This study uses the Streamer radiative transfer model (Key & Schweiger, 1998) to show that the type of aerosol (absorbing versus scattering) and the aerosol optical depth (AOD) can have varying impacts on the MODIS retrievals of cloud optical depth, τ, and effective radius, r_e. Observations from the A-Train satellites in the South Atlantic Ocean from August 2006 to December 2010 show that this effect propagates into the calculation of the cloud droplet number concentration, which uses both τ and r_e from MODIS.

Devasthale & Thomas (2011) examine aerosol overlap events for each season in several latitude bands from 60°N to 60°S using CALIOP Cloud and Aerosol Layer Products. Overlap events show distinct seasonality in different latitude bands around the globe. In 5-10% of all overlap events, the aerosol layer is less than 100 m from the cloud top, potentially leading to cloud-aerosol microphysical interactions. Increasing the aerosol concentration within a liquid water cloud leads to a greater number of smaller cloud droplets. This allows more light to be reflected back to space, causing a net cooling effect, also known as the Twomey effect (Twomey et al., 1984). In the South Atlantic Ocean, in particular, the aerosols often reside several kilometers above the cloud top, and

a wide range of radiative effects have been investigated for this particular scene. Several studies use radiative transfer models to estimate a positive direct effect for the region (Chand et al., 2009; Peters et al., 2011), while Wilcox (2010) suggests a cooling due to the semi-direct effect can counteract the warming effect, depending on the amount of aerosol. The cloud-aerosol interactions in this region are important to the regional climate and their complexity demands further investigation into the accuracy of satellite retrievals of cloud and aerosol properties.

The MODIS retrieval algorithms use combinations of reflectances at water-absorbing and non-absorbing channels to detect cloud optical depth and effective radius. MODIS does not take into account the impact of overlying aerosols on the reflectances at these channels, thus leading to biases in the retrievals. Cattani et al. (2006) model an aerosol layer (AOD = 0.5) above a liquid water cloud, and show that the cloud optical depth retrievals are underestimated by 20-25%. Studies using satellite observations in this region find similar results (Haywood et al., 2004; Meyer et al., 2013). Our study agrees well with these results, suggesting a strong underestimation of cloud optical depth and effective radius in the presence of absorbing aerosols. The magnitude of this effect, however, varies with increasing AOD. We show that scattering aerosols have opposite, but much smaller effects on MODIS retrievals with increasing AOD as well.

Aerosol layers comprised of absorbing or scattering aerosols with varying optical depth above a liquid cloud are modeled, and the TOA reflectances mapped onto a standard LUT. As the AOD increases, the reflectances change drastically for the soot aerosols (absorbing), and vary only slightly for the sulfate aerosols (scattering). Optimal estimation converts these reflectances into cloud optical depths and effective radii. We

show that as the AOD of the soot layer increases to 1, the optical depth is underestimated by up to 60 – 80%. This effect varies between -10 – 10% for the sulfate aerosol layer, depending on the thickness of the cloud below. The effective radius retrievals for the soot layer are complicated by the fact that certain scenes (low cloud optical depth and small effective radius) will not remain on the LUT as the AOD is increased. That is to say that the reflectances at 0.86 μm will become too low for MODIS to recognize them as potential cloud features, and the retrieval will fail. Where reflectances remain on the LUT domain, the effective radius is slightly overestimated, then underestimated with increasing AOD (see Fig. 4.6). For sulfate aerosols, the effective radius is slightly overestimated with increasing AOD by 0 – 10%.

A-Train satellite observations in the South Atlantic Ocean from August 2006 – December 2010 are investigated in this study in order to verify this effect in the observations. Vertical profiles are separated into cases where the aerosol layer is vertically separated from the cloud top, and cases where the aerosol layer is likely touching the cloud top. The cloud droplet number concentrations (N), calculated following the method from Bennartz (2007), incorporate MODIS cloud optical depth and effective radius measurements. We suggest that the observed increase in N for cases when the aerosol layer is not touching the cloud can be attributed to the biases in MODIS optical depth and effective radius. When the aerosol layer is touching the cloud, the trends in N exhibit a combination of the first IAE for AODs < 0.4, and the effect of aerosols on the MODIS retrievals for AODs > 0.4.

Several studies depend on MODIS observations of cloud properties to estimate a net radiative forcing for the region (Chand et al., 2009; Peters et al., 2011). This study

expands upon the work of previous studies, showing that an elevated aerosol layer in the South Atlantic Ocean can have varying impacts on the MODIS retrievals depending on the aerosol type and amount, with soot aerosols accounting for the largest change in MODIS retrievals. Devasthale & Thomas (2011) highlight the significant temporal and spatial differences of aerosol layers residing above liquid water clouds around the world. This study also shows how different atmospheric temperature and humidity profiles affect the retrievals of cloud optical depth and effective radius in a radiative transfer model. Understanding potential errors in MODIS retrievals on the global scale involves expansion of this type of study, including radiative transfer simulations of different cloud-aerosol scenes, different temperature and humidity profiles, and more satellite observations. Further research on this topic will help reduce the large uncertainties associated with cloud and aerosol effects on the global climate.

Appendix A: Symbols

Symbol	Name	Units
β_e	Volume Extinction Coefficient	km^{-1}
β_s	Scattering Coefficient	km^{-1}
β_a	Absorption Coefficient	km^{-1}
ω	Single scatter albedo	-
θ_i	Solar zenith angle	degrees
g	Asymmetry parameter	-
λ	Wavelength	μm
X	Size parameter	-
r	Radius	μm
τ	Cloud optical depth	-
r_e	Cloud effective radius	μm
$I^{\uparrow}$	Radiance at the top of the atmosphere	$W\ m^{-2}\ sr^{-1}$
$r_{0.86} / r_{2.1}$	Reflectances at 0.86 or 2.1 μm	-
F_0	Solar constant	$W\ m^{-2}$
N	Cloud Droplet Number Concentration	cm^{-3}

Appendix B: Acronyms

Acronym	Name
AMSR-E	Advanced Microwave Scanning Radiometer for the Earth Observing System
AOD	Aerosol Optical Depth
AVAC-S	A-Train Validation of Aerosols and Clouds with SEVERI
BC	Black Carbon
CALIPSO	Cloud-Aerosol Lidar and Infrared Pathfinder Satellite Observation
CALIOP	Cloud-Aerosol Lidar with Orthogonal Polarization
CCN	Cloud Condensation Nuclei
CPR	Cloud-Profiling Radar
CTT	Cloud Top Temperature
CTH	Cloud Top Height
EUMETSAT	European Organisation for the Exploitation of Meteorological Satellites
IAE	Indirect Aerosol Effect
IR	Infrared
LUT	Lookup Table
LWP	Liquid Water Path
MODIS	Moderate Resolution Imaging Spectroradiometer
MSG	Meteosat Second Generation
OE	Optimal Estimation
OPAC	Optical Properties of Aerosols and Clouds
PAOD	Proxy Aerosol Optical Depth
TAB	Total Attenuated Backscatter
TOA	Top of Atmosphere
SEVERI	Spinning Enhanced Visible and InfraRed Imager

REFERENCES

Bennartz, R. (2007). Global assessment of marine boundary layer cloud droplet number concentration from satellite. *Journal of Geophysical Research*, *112*(D2), D02201. doi:10.1029/2006JD007547

Boucher, O., D. Randall, P. Artaxo, C. Bretherton, G. Feingold, P. Forster, V.-M. Kerminen, Y. Kondo, H. Liao, U. Lohmann, P. R., & S. K. Satheesh, S. Sherwood, B. S. and X. Y. Z. (2013). Clouds and Aerosols. *Climate Change 2013: The Physical Science Basis. Contribution of Working Group I to the Fifth Assessment Report of the Intergovernmental Panel on Climate Change*, (January 2014).

Cattani, E., Costa, M. J., Torricella, F., Levizzani, V., & Silva, a. M. (2006). Influence of aerosol particles from biomass burning on cloud microphysical properties and radiative forcing. *Atmospheric Research*, *82*(1-2), 310–327. doi:10.1016/j.atmosres.2005.10.010

Chand, D., Wood, R., Anderson, T. L., Satheesh, S. K., & Charlson, R. J. (2009). Satellite-derived direct radiative effect of aerosols dependent on cloud cover. *Nature Geoscience*, *2*(3), 181–184. doi:10.1038/ngeo437

Devasthale, A., & Thomas, M. A. (2011). A global survey of aerosol-liquid water cloud overlap based on four years of CALIPSO-CALIOP data. *Atmospheric Chemistry and Physics*, *11*(3), 1143–1154. doi:10.5194/acp-11-1143-2011

Ellingson, R.G, Ellis, J., Fels, S. (1991a). The intercomparison of radiation codes used in climate models: long wave results. *J. Geophys. Res.*, *96*, 8929–8953.

Ellingson, R.G, Ellis, J., Fels, S. (1991b). The intercomparison of radiation codes used in climate models: long wave results. *J. Geophys. Res.*, *96*, 8929–8953.

Forster, P., V. Ramaswamy, P. Artaxo, T. Berntsen, R. Betts, D.W. Fahey, J. Haywood, J. Lean, D.C. Lowe, G. Myhre, J. Nganga, R. P., & G. Raga, M. S. and R. V. D. (2007). Changes in Atmospheric Constituents and in Radiative Forcing. *Climate Change 2007: The Physical Science Basis. Contribution of Working Group I to the Fourth Assessment Report of the Intergovernmental Panel on Climate Change*.

Haywood, J. M., Osborne, S. R., & Abel, S. J. (2004). The effect of overlying absorbing aerosol layers on remote sensing retrievals of cloud effective radius and cloud optical depth. *Quarterly Journal of the Royal Meteorological Society*, *130*(598), 779–800. doi:10.1256/qj.03.100

Hess, M., Koepke, P., & Schult, I. (1998). Optical Properties of Aerosols and Clouds: The Software Package OPAC. *Bulletin of the American Meteorological Society*, *79*(5), 831–844.

Hobbs, P. V. (2002). Clean air slots amid atmospheric pollution. *Nature*, *415*(February), 861.

Johnson, B. T., Shine, K. P., & Forster, P. M. (2004). The semi-direct aerosol effect: Impact of absorbing aerosols on marine stratocumulus. *Quarterly Journal of the Royal Meteorological Society*, *130*(599), 1407–1422. doi:10.1256/qj.03.61

Key, J. R., & Schweiger, A. J. (1998). Tools for atmospheric radiative transfer: Streamer and FluxNet. *Computers & Geosciences*, *24*(5), 443–451. doi:10.1016/S0098-3004(97)00130-1

Liu, Z., Omar, A. H., Yongxiang, H., Vaughan, M. A., & Winker, D. M. (2005). CALIOP Algorithm Theoretical Basis Document Part 3 : Scene Classification Algorithms, (October), 1–56.

Lu, M.-L., & Seinfeld, J. H. (2006). Effect of aerosol number concentration on cloud droplet dispersion: A large-eddy simulation study and implications for aerosol indirect forcing. *Journal of Geophysical Research*, *111*(D2), D02207. doi:10.1029/2005JD006419

Meyer, K., Platnick, S., Oreopoulos, L., & Lee, D. (2013). Estimating the direct radiative effect of absorbing aerosols overlying marine boundary layer clouds in the southeast Atlantic using MODIS and CALIOP. *Journal of Geophysical Research: Atmospheres*, *118*(10), 4801–4815. doi:10.1002/jgrd.50449

Peters, K., Quaas, J., & Bellouin, N. (2011). Effects of absorbing aerosols in cloudy skies: a satellite study over the Atlantic Ocean. *Atmospheric Chemistry and Physics*, *11*(4), 1393–1404. doi:10.5194/acp-11-1393-2011

Petty, G. (1999). *Review of Retrieval and Analysis Methods for Passive Microwave Imagers, In Microwave Radiometery for Atmospheric Research and Monitoring, report of the COST 712 action, ESA/ESTEC* (pp. 3–29).

Petty, G. (2006). *A First Course in Atmospheric Radiation* (2nd ed.). Madison, WI: Sundog Publishing.

Platnick, S., King, M. D., Ackerman, S. A., Menzel, W. P., Baum, B. A., Riédi, J. C., & Frey, R. A. (2003). The MODIS Cloud Products : Algorithms and Examples From Terra, *41*(2), 459–473.

Poulsen, C. a., Siddans, R., Thomas, G. E., Sayer, a. M., Grainger, R. G., Campmany, E., … Watts, P. D. (2012). Cloud retrievals from satellite data using optimal estimation: evaluation and application to ATSR. *Atmospheric Measurement Techniques*, *5*(8), 1889–1910. doi:10.5194/amt-5-1889-2012

Raschke, E. (1996). *Radiation and Water in the Climate System*. Berlin ; New York: Springer.

Roberts, G., Wooster, M. J., & Lagoudakis, E. (2009). Annual and diurnal african biomass burning temporal dynamics. *Biogeosciences*, *6*(5), 849–866. doi:10.5194/bg-6-849-2009

Rodgers, C. D. (2000a). *Inverse Methods for Atmospheric Sounding*. Singapore: World Scientific.

Rodgers, C. D. (2000b). *Inverse Methods for Atmospheric Sounding*. Singapore: World Scientific.

Stephens, G. L., Vane, D. G., Boain, R. J., Mace, G. G., Sassen, K., Wang, Z., … CloudSat Science Team, T. (2002). The CloudSat Mission and the A-Train: A New Dimension of Space-Based Observations of Clouds and Precipitation. *Bulletin of the American Meteorological Society*, *83*(12), 1771–1790. doi:10.1175/BAMS-83-12-1771

Twomey, A., Piepgrass, M., & Wolfe, T. L. (1984). An assessment of the impact of pollution on global cloud albedo, *360*, 356–366.

Vaughan, M. A., Winker, D. M., & Powell, K. A. (2005). CALIOP Algorithm Theoretical Basis Document Part 2 : Feature Detection and Layer Properties Algorithms, (September), 1–87. Retrieved from http://www-calipso.larc.nasa.gov/resources/pdfs/PC-SCI-202_Part2_rev1x01.pdf

Wilcox, E. M. (2010). Stratocumulus cloud thickening beneath layers of absorbing smoke aerosol. *Atmospheric Chemistry and Physics*, *10*(23), 11769–11777. doi:10.5194/acp-10-11769-2010

Wilcox, E. M. (2012). Direct and semi-direct radiative forcing of smoke aerosols over clouds. *Atmospheric Chemistry and Physics*, *12*(1), 139–149. doi:10.5194/acp-12-139-2012

Wood, R. (2012). Stratocumulus Clouds. *Monthly Weather Review*, *140*(8), 2373–2423. doi:10.1175/MWR-D-11-00121.1